UNCLASSIFIED

SECURITY CLASSIFICATION OF THIS PAGE *(When Data Entered)*

REPORT DOCUMENTATION PAGE	READ INSTRUCTIONS BEFORE COMPLETING FORM
1. REPORT NUMBER NAVENVPREDRSCHFAC Contractor Report CR 84-04	2. GOVT ACCESSION NO. / 3. RECIPIENT'S CATALOG NUMBER
4. TITLE *(and Subtitle)* Cloud Bands Structure of Hurricane David, 1979 - A Case Study	5. TYPE OF REPORT & PERIOD COVERED: Final 6. PERFORMING ORG. REPORT NUMBER
7. AUTHOR(s) Francis H. Nicholson	8. CONTRACT OR GRANT NUMBER(s): N62271-81-M-2095
9. PERFORMING ORGANIZATION NAME AND ADDRESS Systems Control Technology, Inc. Palo Alto, CA 94303	10. PROGRAM ELEMENT, PROJECT, TASK AREA & WORK UNIT NUMBERS: PE 62759N PE WF59-551 TA 2 NEPRF WU 6.2-17
11. CONTROLLING OFFICE NAME AND ADDRESS Naval Air Systems Command Department of the Navy Washington, DC 20361	12. REPORT DATE: June 1984 13. NUMBER OF PAGES: 46
14. MONITORING AGENCY NAME & ADDRESS *(if different from Controlling Office)* Naval Environmental Prediction Research Facility Monterey, CA 93943	15. SECURITY CLASS. *(of this report)*: UNCLASSIFIED 15a. DECLASSIFICATION/DOWNGRADING SCHEDULE

16. DISTRIBUTION STATEMENT *(of this Report)*

Approved for public release; distribution is unlimited.

17. DISTRIBUTION STATEMENT *(of the abstract entered in Block 20, if different from Report)*

18. SUPPLEMENTARY NOTES

19. KEY WORDS *(Continue on reverse side if necessary and identify by block number)*

Cloud spiral bands
Tropical cyclone
Intensity

20. ABSTRACT *(Continue on reverse side if necessary and identify by block number)*

The nature of the spiral banding of Hurricane David immediately before, during, and after a period of intensification is examined. The tropical cyclone spiral banding features are analyzed by the Tactical Environmental Display System (TEDS) program on the NAVENVPREDRSCHFAC Satellite-data Processing and Display System (SPADS). Results show that a secondary energy maximum exists in the spiral spectrum during the hurricane's intensification period, and that the behaviors of the eye do not seem to correlate with the intensification of the storm.

DD FORM 1 JAN 73 1473 EDITION OF 1 NOV 65 IS OBSOLETE
S/N 0102-014-6601

UNCLASSIFIED

SECURITY CLASSIFICATION OF THIS PAGE *(When Data Entered)*

CONTENTS

AN (1) AD-A144 529
FG (2) 040200
CI (3) (U)
CA (5) SYSTEMS CONTROL TECHNOLOGY INC PALO ALTO CA
TI (6) Cloud Bands Structure of Hurricane David, 1979 - A Case Study.
TC (8) (U)
DN (9) Final rept.,
AU (10) Nicholson,F. H.
RD (11) Jun 1984
PG (12) 47p
CT (15) N00221-81-M-2095
PJ (16) F59551
TN (17) WF595512
RN (18) NEPRF-CR-84-04
RC (20) Unclassified report
DE (23) *Hurricanes, *Clouds, Shape, Bands(Strips), Variations, Statistical analysis
DC (24) (U)
ID (25) TEDS(Tactical Environmental Display System), Hurricane David, PE62759N, WU0217
IC (26) (U)
AB (27) The nature of the spiral banding of Hurricane David immediately before, during, and after a period of intensification is examined. The tropical cyclone spiral banding features are analyzed by the Tactical Environmental Display System (TEDS) program on the NAVENVPREDRSCHFAC Satellite-data Processing and Display System (SPADS). Results show that a secondary energy maximum exists in the spiral spectrum during the hurricane's intensification period, and that the behaviors of the eye do not seem to correlate with the intensification of the storm. (Author)
AC (28) (U)
DL (33) 01
SE (34) F
CC (35) 412500

NAVENVPREDRSCHFAC
CONTRACTOR REPORT
CR 84-04

LIBRARY
RESEARCH REPORTS DIVISION
NAVAL POSTGRADUATE SCHOOL
MONTEREY, CALIFORNIA 93943

NAVENVPREDRSCHFAC CR 84-04

CLOUD BANDS STRUCTURE OF HURRICANE DAVID, 1979 – A CASE STUDY

Prepared By:

Francis H. Nicholson
Systems Control Technology, Inc.
Palo Alto, CA 94303

Contract No. N62271-81-M-2095

JUNE 1984

Prepared For:
NAVAL ENVIRONMENTAL PREDICTION RESEARCH FACILITY
MONTEREY, CALIFORNIA 93943

1. Introduction

Background

The purpose of this study is to explore the nature of the spiral banding of Hurricane David immediately before, during and after a period of intensification. The satellite IR data of Hurricane David's spiral bands are extracted and analyzed by the Tactical Environmental Display System (TEDS) program on the NAVENVPREDRSCHFAC satellite data processing computer SPADS. The details of the TEDS developed by Nicholson in 1983 are documented by Cook (1984) and are not repeated here. However, it suffices to state that the object of TEDS is to sample satellite data from the spiral coordinates orthogonal to the tropical cyclone spiral bands. TEDS also performs Fourier analysis over the satellite data along each of the 10 spiral bands illustrated in Fig. 1. In this study, the satellite IR data and the analyzed Fourier components are considered together to assess the behavior of hurricane David's cloud bands over his intensification period.

Theoretical Considerations

There are three significant points which need to be addressed in consideration of the banded structure of tropical and extratropical storms. These points are:

1) Band Length
2) Band distribution for non-intensifying but stable cyclones
3) Band distribution for intensifying storms.

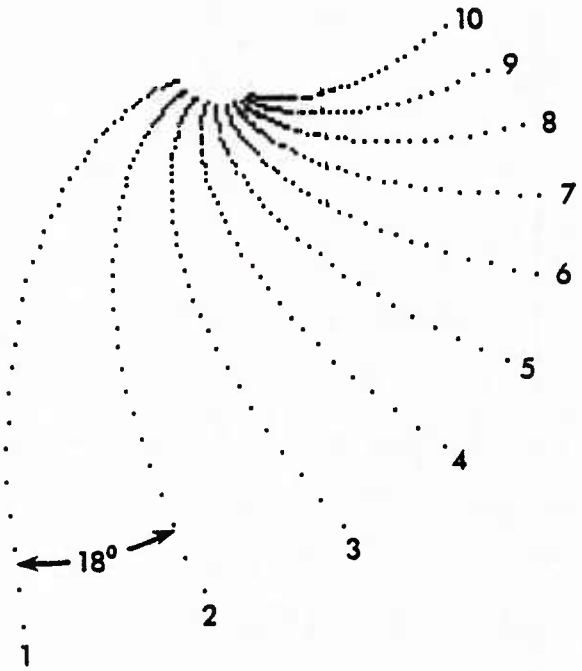

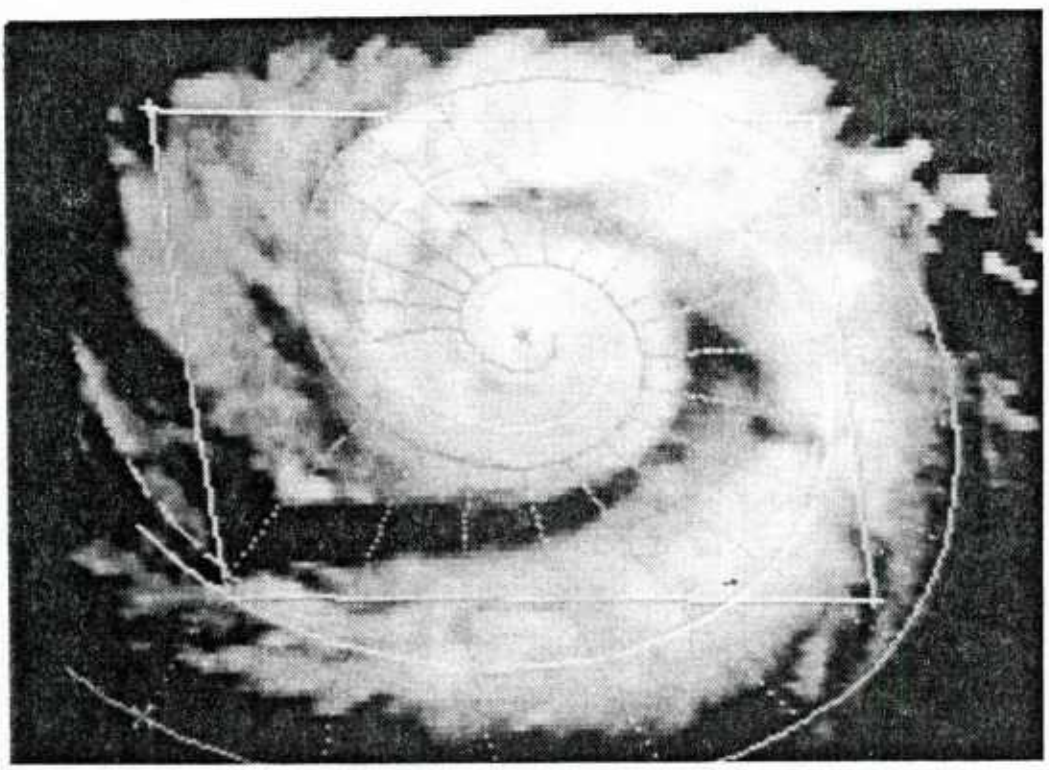

Figure 1. The dots represent a typical spiral analysis grid used in this study. Each dot represents a datum sampling point. The grid consists of ten diverse spiral rows of data points which have a common center (not shown) and are orthogonal to the cloud bands. Each spiral has the same inflow angle and is separated from its neighbors by 18°.

The first of these, band length, is a measure of band extent as a function of wave number compatible with the specification that the underlying divergence field satisfies Laplace's equation (Nicholson 1983). The wave number of the band is such that, if all of the bands were to start at the center of the storm with a given amplitude, A, then the lateral extent, or length of the bands themselves, would be given by exp(A/n) where n is the wave number. The higher the wave number, the shorter the band. Band No. 1 may have an extent of two thousand miles, (Fig. 1 and 2), whereas band No. 2 barely reaches fifty. Thus the extent decreases until band eight barely reaches three miles long. All other things being equal, the hurricane should be highly asymmetric with one spiral band extending much further out than all the others, and small bands of high frequency confined to the innermost storm, both of which phenomena are regularly observed.

The second consideration is the role of the pressure asymmetries accompanying the bands. In axially symmetric vortices there can be no pressure torque which azimuthally averages to a non zero value. This is not the case with spiral asymmetric pressure fields. The azimuthal average is non zero so that the pressure torque plays a vital role in concentrating the vortex energetics by allowing high winds to penetrate towards the center of the vortex. Instead of angular momentum being reduced by diminishing the winds, the winds may actually increase, but through the pressure torque it is the radius of the winds which decreases. The distribution of energetics of the vortex is such that the greatest energy is produced near the center of the vortex. The presence of spiral bands seems to be the sine qua non for the intensification of vortices all the way from waterspouts to tornadoes and hurricanes. Well defined bands and the extent of their winding are documented by Fett (1973) in extratropical storms of unusual intensity.

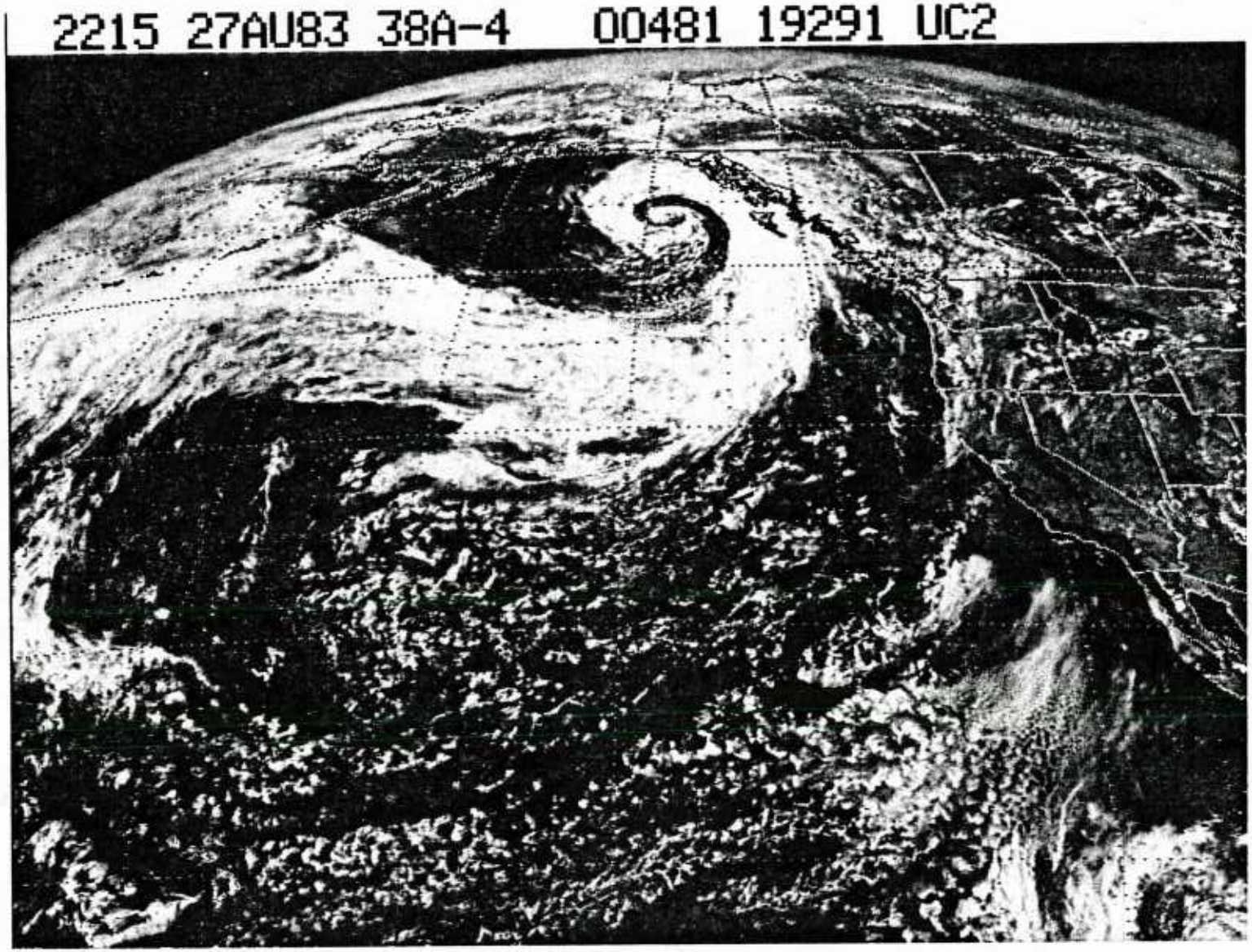

Fig. 2: Example of the extent of Band No. 1 in an extra-tropical cyclone.

In order for the spiral pressure asymmetries to satisfy the condition that the torque be independent of radius, we shall see that the peak of the spiral spectrum must be given by the cosecant of the inflow angle of the spiral bands into the center of the storm. This is difficult to measure with great accuracy, partly because the individual bands do not share the same center either with bands of different wave number or with the center of the symmetric vortex, and partly because the bands do not share the same extent. Thus bands of wave number eight appear only near the center of the storm, whereas band two lies predominantly in the periphery before being masked in the interior by higher frequency bands, and band one may extend up to a thousand miles beyond the rest of the storm proper. Since the inflow angle typically varies between 20 and 45 degrees, the spectral peak usually occurs between wave number one and a half and two. That is to say, that most of the spectral energy falls into wave one, about half as much into two and the rest is accounted for by cumulus and pixel noise.

The third consideration is that a bimodal distribution occurs in hurricane David manifest by a strong peak centered about wave numbers 7-8 as well as the initial waves, 1 and 2. This implies a regional, if not a local torque in the interior which may indicate the evolution of the vortex from the complex two part vortex to the mature, three part vortex, complete with eye and always characterized by marked spiral banding. The vortex subsequently settles into the mature mode, which, with the spiral asymmetries described above, constitutes the composite vortex described by Nicholson (1983). We will now consider the three points presented above in greater detail.

2. Methodology - Analytical Analysis

Spiral Band

In order to determine the extent of the spiral bands it is important to understand the rationale for the existence of spiral bands. It is postulated (Nicholson, 1983) the divergence field is governed by

$$\nabla_2^2 \delta = 0, \infty.$$

where δ is the two dimensional horizontal divergence. The infinity sign means that the Laplacian, the average value of a point with its neighbors, is undefined. At a boundary, the point lacks neighbors and therefore is undefined. Any finite field must have boundaries. Laplace's equation is a second order, linear, homogeneous partial differential equation with solutions entirely determined by boundary conditions. Since, by definition, boundaries are implied, the infinity sign is virtually tautological for a finite phenomenon satisfying Laplace's equation.

In cylindrical coordinates Laplace's equation is given by

$$\frac{1}{r^2}\left(\frac{\partial^2}{\partial\, \ell n\, r^2} + \frac{\partial^2}{\partial \theta^2}\right) \delta = 0$$

and solutions to Laplace's equation are either linear in $\ell n\, r$ or θ or an exponential of any complex combination of the two. Thus, $\exp(n(\theta + i\, \ell n\, r)e^{i\alpha})$ is a solution where n is a wave number and $e^{i\alpha}$ is a versor. The versor rotates the semilog coordinates $\theta + i\ell nr$ through the angle, α, to produce new log spiral coordinates. Thus the solution is given by

$$\delta = \sum_{n=1}^{\infty} \gamma(n)\ e^{n(S_\theta + i\, S_r)}$$

where $S_\theta + iS_r = (\theta + i\ell n\ r)e^{i\alpha}$ and S_θ and iS_r are the orthogonal spiral coordinates. By Euler's equation

$$e^{n(S_\theta + iS_r)} = e^{nS_\theta}(\cos n S_r + i \sin n S_r).$$

The real part is given by

$$\gamma(n)e^{nS_\theta} \cos n S_r .$$

To determine the amplitude, $\gamma(n)$, Fourier analysis requires samples to be taken at equal, regular intervals of ΔS_r up to 2N where N is the highest frequency. This being the case, the actual spatial samplings must be done in exponential intervals of $e^{i\Delta S_r}$ where S_r varies between 0 and $2\pi \sin \alpha$.

Typically, a sine wave in the divergence field is stretched along e^{S_r}. Fig. 3 is two different representations of the same phenomenon. Figure 3.b indicates the spatial bias of the sine wave. This difference is manifest in the spectral distribution of the individual amplitudes. There is a strong difference in the spectra compiled by Fourier analysis based on exponential versus linear sampling. Because of this direction, the analysis described by this paper is based on exponential sampling (Fig. 3.b). A peak in exponential sampling would be substantially smoothed in linear sampling, and vice-versa. The distinction is essential in order to determine the noise to signal ratio, an important consideration in the validity of a series solution manifest in natural phenomena. It is the intent of the study to match the analytical solution (Laplace's solution with the phenomenon (hurricane spiral cloud bands)) displayed by the satellite data.

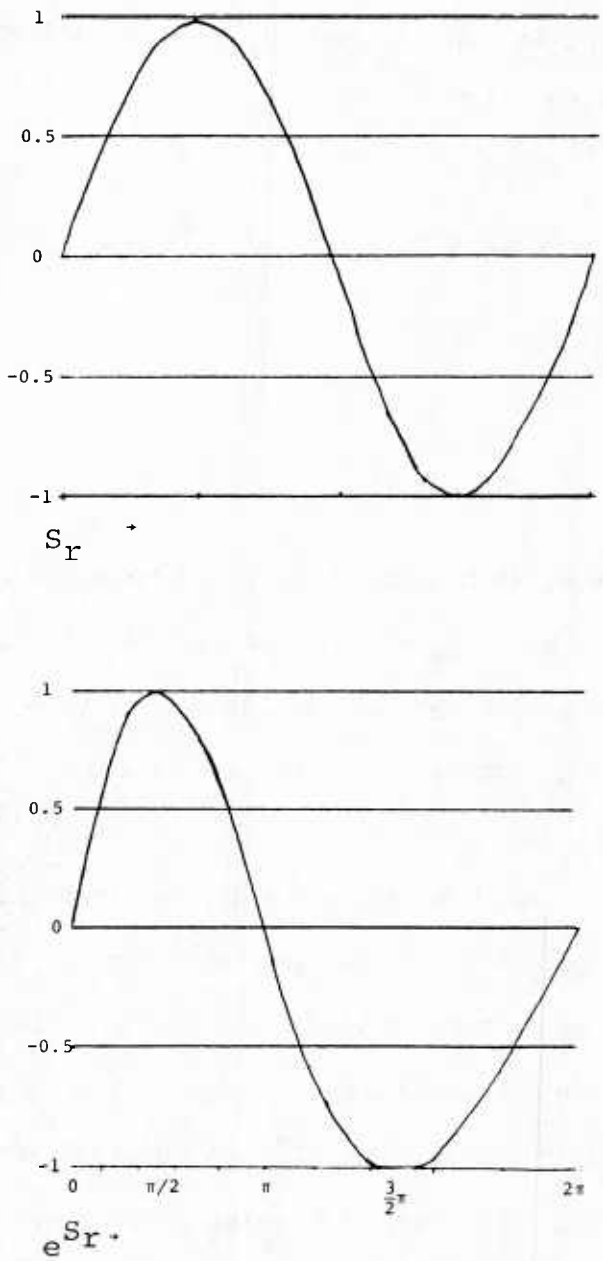

Fig. 3 a) Ordinary sine wave as a function of the exponent of the real space coordinate, i.e. S_r. The undistorted sine wave exhibits symmetry lacking in the skewed wave in the graph below. b) Distribution of values of sine wave plotted in real space, e^{S_r}, though a function of S_r. Note the broadening of the wave with increase in values of S_r. The first half of the wave is crowded into the first third of the wave length, the second half is spread over the remaining two thirds, becoming progressively broader with higher values.

The length of a given band is determined by its initial amplitude and its wave number. In Fig. 4 waves one through four are plotted with the ordinate representing the logarithm of the divergence field and the abscissa the azimuthal extent occupied by the band. Since $\delta = \gamma_0(n)\, e^{-nS_\nu} \cos n S_r$ and $S_\nu = \nu \csc \alpha$, then $\ell n \delta = \ell n \gamma_0 (n) - n \nu \csc \alpha$ where n is the slope of the band. The greater the wave number, or slope, the shorter the projection on ν. Assuming all of the bands begin with the same initial amplitude, then the semilog projection of the band length is given by $\gamma_0(n)/n$ in terms of ν. The actual band length, however, is given by $\exp(\gamma_0(n)/n)$. Table 1 indicates the bandlength for $\gamma_0(n) = 7.5$ for a number of waves.

TABLE I

Wave Number	Length
1	2321.6 (n. mi)
2	47.942
3	13.197
4	6.889
5	4.711
7	3.03
8	2.63

For higher wave numbers to appear means a significant shift in the patterns of the energetics. The initial amplitude of the higher wave numbers must be correspondingly greater to show up in the IR.

Azimuthally Averaged Spiral Pressure Torque

In this section we will discuss the asymmetric, azimuthally averaged spiral pressure torque. We shall see that the azimuthally averaged spiral pressure asymmetries produces a negative pressure torque, possibly sufficient to reduce the radii of inspiralling air to small values yet keeping the velocity value of the inspiralling air at high levels. Thus both the energetics and the angular momentum budgets are accommodated. In the section following there will be a

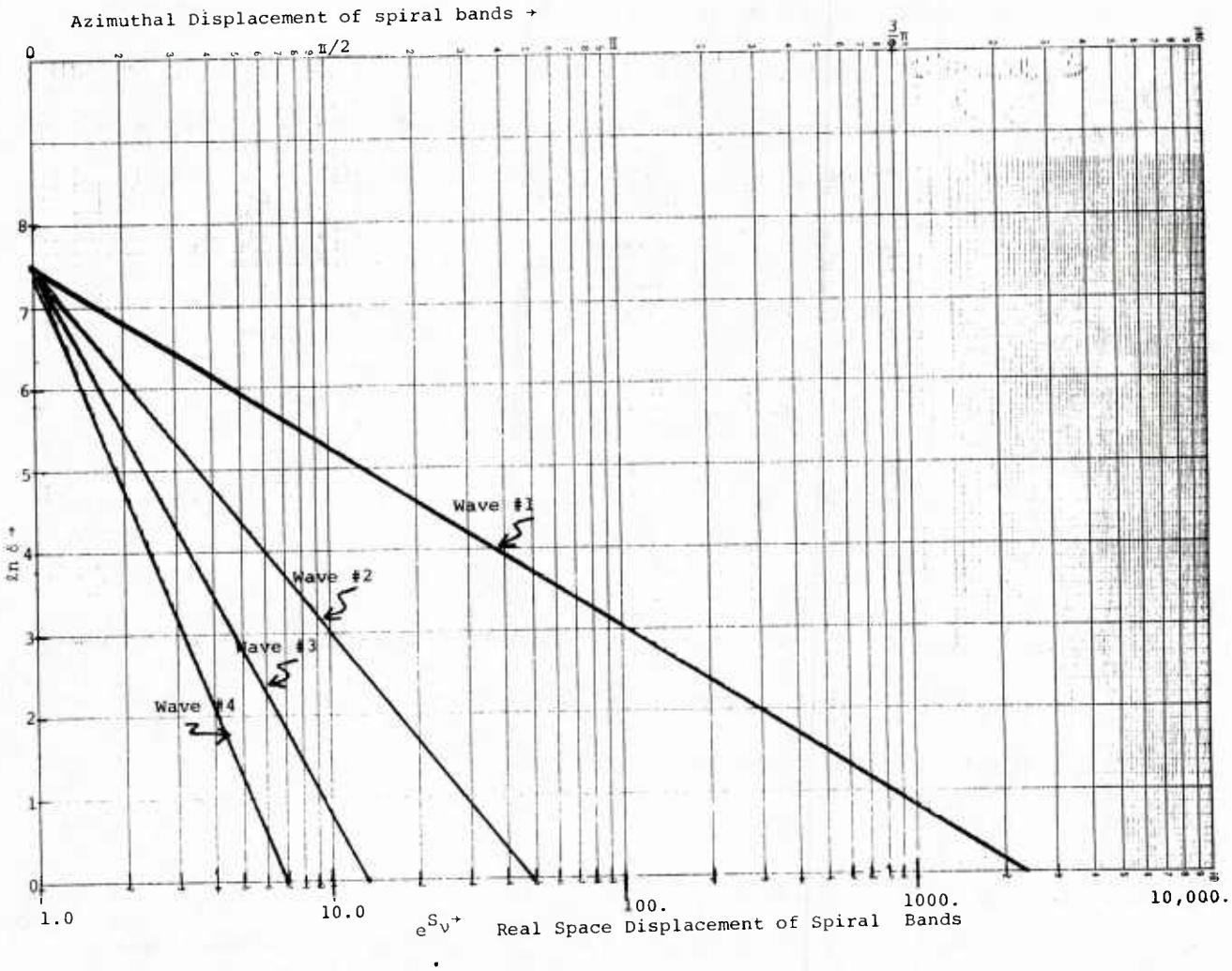

Fig. 4. Plot of logarithm of the divergence field vs. the corresponding spiral length. The azimuthal displacement of the spiral band in directly proportional to the logarithm of the spiral length. Therefore a plot of the logarithm of the divergence field strength vs. azimuth also indicates the length of the band in semilog coordinates.

discussion of the introduction of higher wave numbers in a bimodal spectral peak, thereby introducing a very high torque in the central part of the storm, possibly resulting in the creation of a new regime, the core of the mature vortex. As often as not, the eye of the symmetric storm is offset from the center of the spiral so that the spiral center and axially symmetric center are not coincident.

From the observations, we find that rarely does the spiral center coincide with the eye. As discussed above, this is to prevent negative spiral torques from counteracting the positive torque of the eye. This torque produces supergradient winds allowing for low level divergence in the eye. In Fig. 5 it can be seen that the axially symmetric frictional torque is directly proportional to the slope of the vorticity field; the frictional torque is a positive constant in the eye, strong and negative constant in the wall cloud and weak and negative in the outer regime.

By destroying angular momentum, the amount of work needed to import air to the center of the storm is decreased. Both spiral frictional and pressure torques counteract eye torque and probably sustain and enhance wall cloud torque. Offset spiral and axial centers prevent counteraction of eye torque.

A partial representation of the angular momentum equation is given below:

$$\underset{\sim}{r} \times \frac{\partial \vec{V}}{\partial t} = \ldots \underset{\sim}{r} \times -\alpha \nabla p, \qquad (1)$$

where $\underset{\sim}{r}$ is the radial arm, $\underset{\sim}{V}$, the velocity vector and $-\alpha\nabla p$ the pressure gradient force. Assuming, as a first approximation that α , the specific volume of air, is constant, the vertical component of (1) may be rewritten as

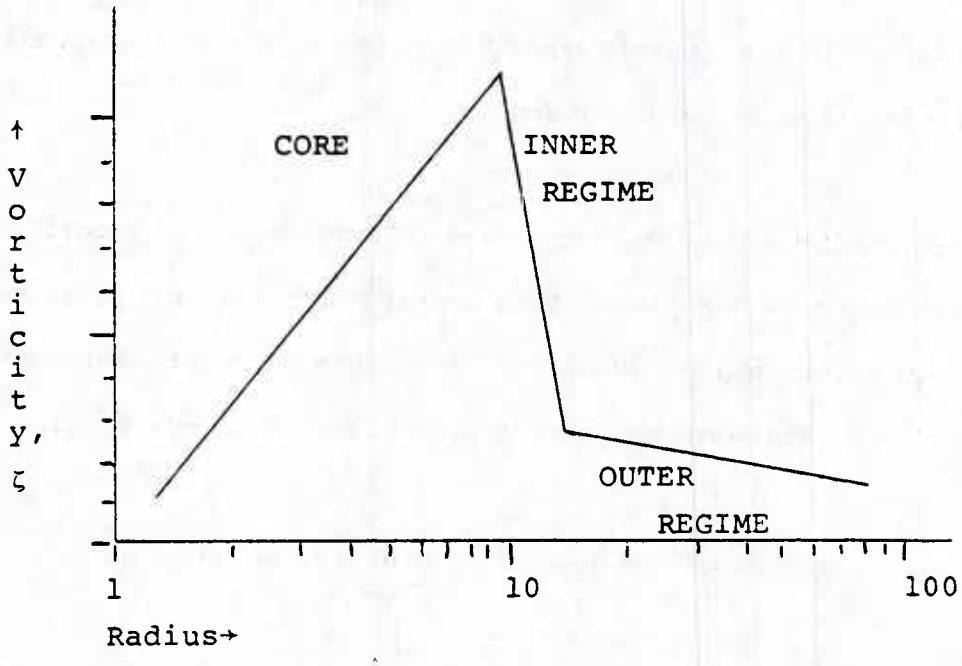

Fig. 5. Piecewise, continuous distribution of vorticity showing core, inner and outer regimes. Since vorticity is linear in the logarithm of the radius, it satisfies Laplace's equation. Sine $F = \partial\zeta / \partial r$ and $rF = \partial\zeta / \partial \ln r$, then the slope of the vorticity is proportional to the frictional torque.

$$\frac{\partial g}{\partial t} = \ldots \underset{\sim}{r} \times - \frac{\alpha \partial p}{r \partial \theta}$$

$$= - \alpha \frac{\partial p}{\partial \theta}, \quad \text{where g is the angular momentum.}$$

Integration over 2 radians obtains

$$\int_0^{2\pi} \partial g/\partial t \, r \, d\theta = -\alpha r p \Big|_0^{2\pi}.$$

But $p = p_0 e^{n(S_\theta + i S_r)} = p_0 e^{n(\theta \cos\alpha - \ell n\, r \sin\alpha + i(\ell n\, r \cos\alpha - \theta \sin\alpha))}$

So $p\Big|_0^{2\pi} = p_0 \exp(n(2\pi \cos\alpha - \ell n\, r \sin\alpha + i(\ell n\, r \cos\alpha - 2\pi \sin\alpha))$
$- p_0 \exp(-n(\ell n\, r \sin\alpha + i\, \ell n\, r \cos\alpha))$.

Taking the real part Re{$\partial g/\partial t$} we obtain

$$\int_0^{2\pi} \partial g/\partial t \; r \, d\theta = - \alpha r p_0 e^{n(2\pi \cos\alpha - \ell n\, r \sin\alpha)} + \alpha r p_0 e^{-n \ell n\, r \sin\alpha} \qquad (2)$$

or

$$= \alpha r p_0 r^{-n \sin\alpha} (1 - e^{n 2\pi \cos\alpha})$$

$$= \alpha p_0 r^{1-n \sin\alpha} (1 - e^{n 2\pi \cos\alpha}). \qquad (3)$$

For the pressure torque to be independent of radius then (3) reduces to $\alpha p_0 (1 - e^{2\pi \cot\alpha})$ when $n = \csc\alpha$.

Thus, in conformity with the general principal that the torque be independent of radius, as stated in Nicholson (1983) the spectral maximum must be determined by the cosecant of the inflow angle of the spiral bands. Since this angle is ordinarily between 20 and 45 degrees, then the spectral maximum must fall between one and three. Thus the predominant wave number in the steady

state tropical storm lies between one and three. The cosecant of 20 degrees is slightly less than three, and the cosecant of 45 degrees is approximately 1.3.

When the torque due to the spiral asymmetries is not independent of radius, then (3) tells us that for low values of n the amplitude is small but the extent of influence is large. Higher n's have greater amplitudes but smaller areas of influence. Pressure torque destroys angular momentum. A shift in the spectrum to 8 provides considerable torque in the region of the wall cloud.

3. Case Study of Intensification of David

Before a detailed analysis of the spectral distribution of hurricane David is presented it would be worthwhile to assess the three kinds of signal obtained by the spiral analysis technique. The reader will notice that the points of sampling (Fig. 1.a) are closer together in the upper portion of the figure, and more separated in the lower part of the picture. This is consistent with the samplings being taken at exponential intervals along the orthogonal dotted spirals. By this means a Fourier analysis of the spiral spectra may be made, in spiral coordinates.

Figure 6 shows an example of the first type of non-spiral noise in the satellite representation, that due to the graininess of individual cumulus elements. This signal appears as high frequency noise in the original analysis with peaks toward the upper end of the range. This sort of signal is amenable to filtering and may be omitted in a reconstruction of the spiral signal, a mathematical reconstruction of the banding of the storm. Another kind of signal appears in Fig. 7 and 8. Fig. 7 is a close up of the center of David. This close up shows the boxiness of the pixels. Near the center of the storm the pixels are sampled so close together that some of the elements are

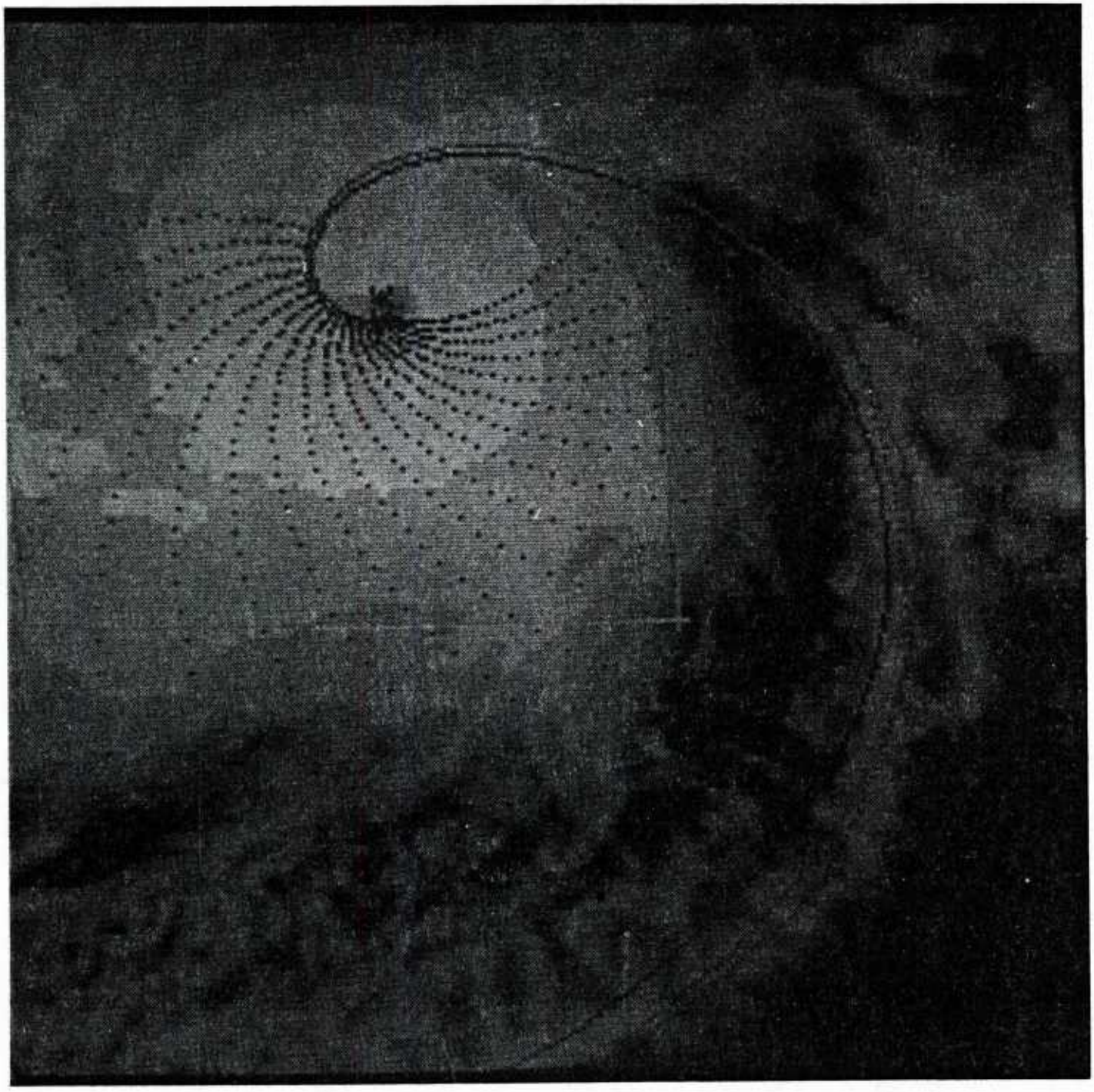

Fig. 6 Noise due to graininess of individual cumulus elements.

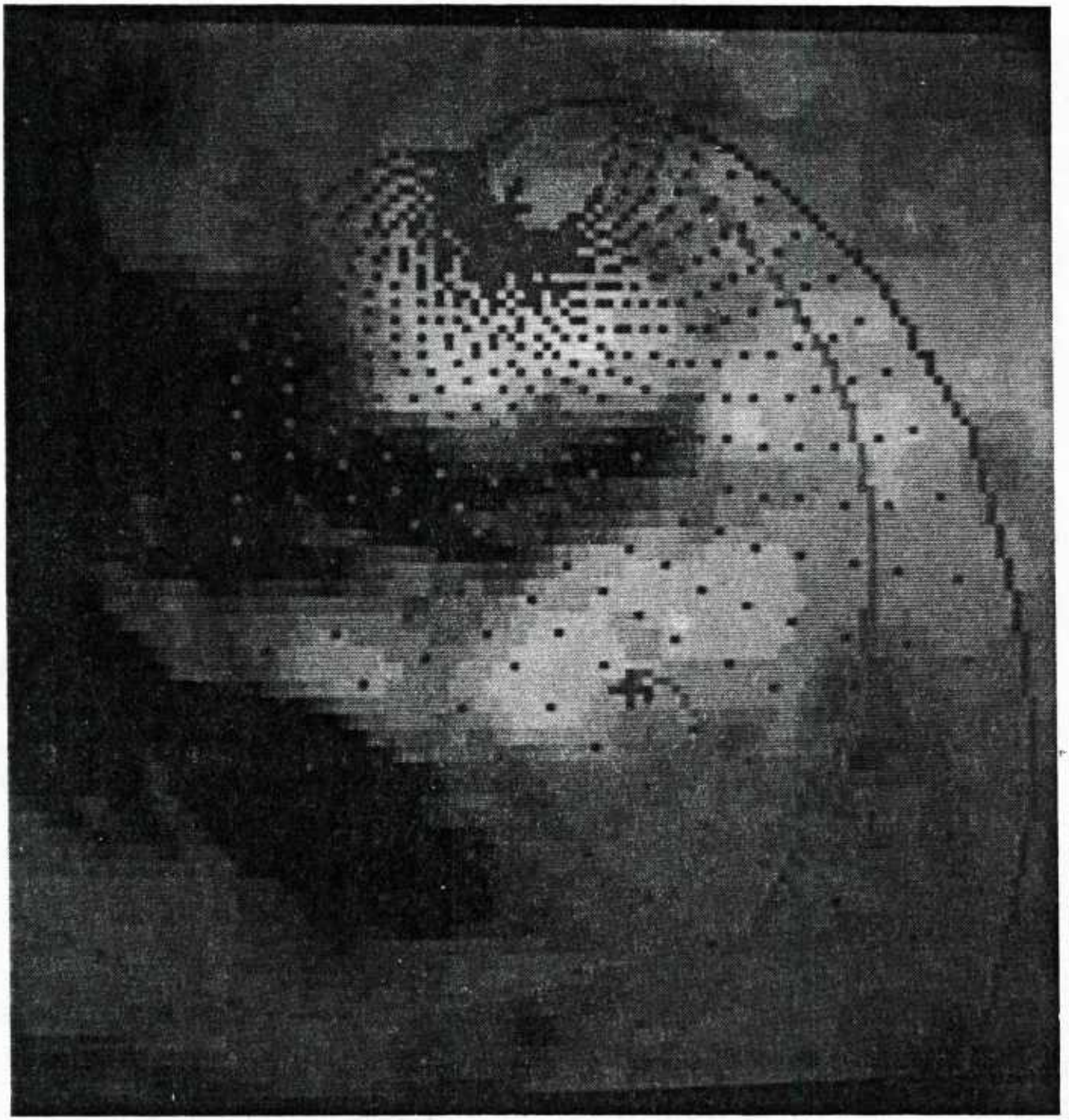

Fig. 7 Noise due to pixel boxiness. Twice magnification of the 2 n mi IR resulotion satellite picture on Hurricane David.

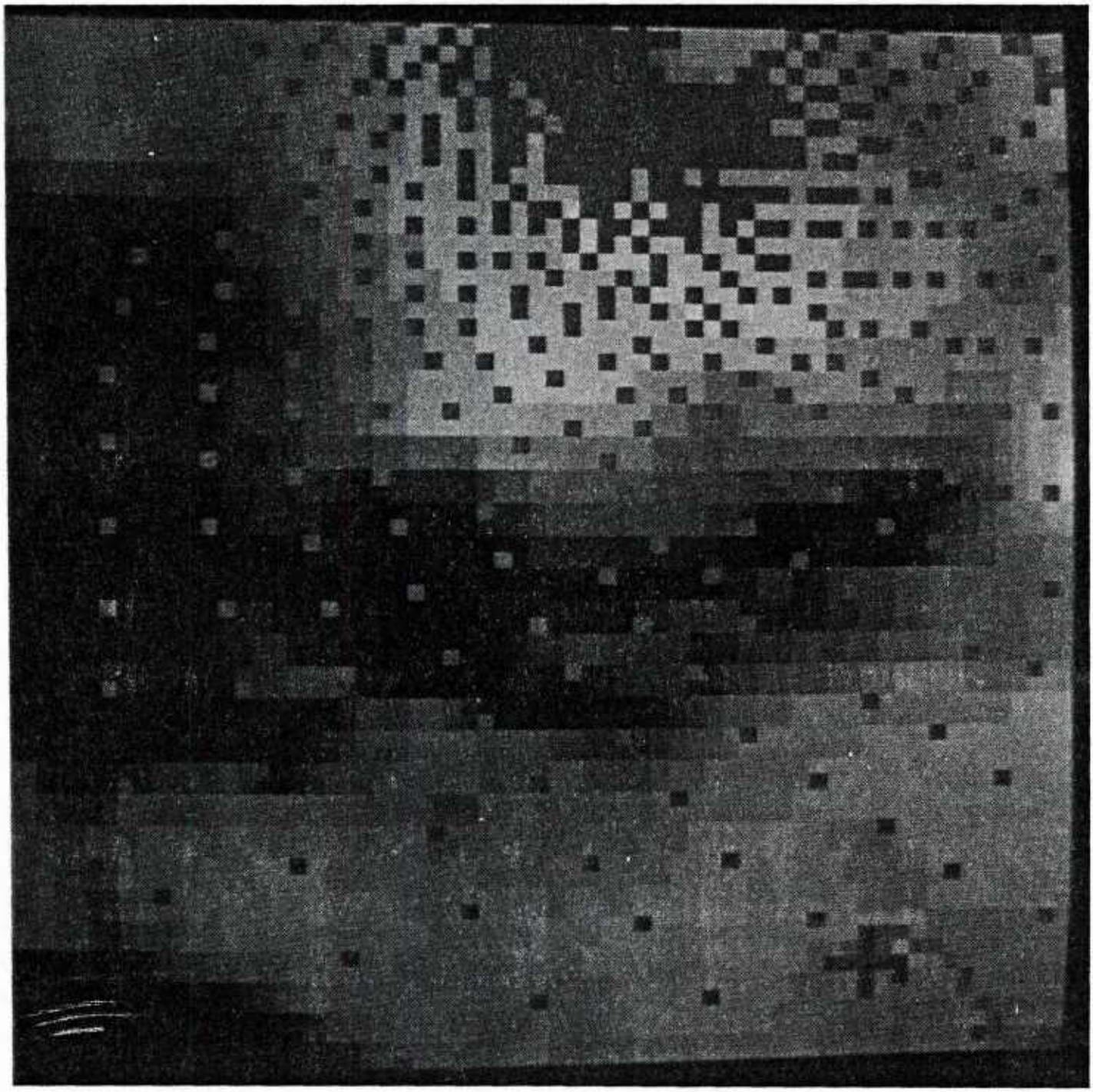

Fig. 8 Similar to Fig. 7, except for eight times magnification.

sampled more than once. This introduces an element of noise into the ultimate Fourier analysis. This element is an attempt by the Fourier analysis to account for the boxiness of the pixels. Fig. 8 is an eight times magnification of David representation.

Thus, it can be seen that it is important to separate out signals from non-banding sources, such as cumulus elements and pixel boxiness from actual banding spectral characteristics.

Fig. 9 - 18 (Appendix) are histograms representing the spiral spectra of the illustrations in Fig. 19 - 28 (Appendix). Fig. 9 matches Fig. 19. The former is the histogram of the spiral analysis given at 14Z 24 Aug 79 (Julian date 238.14), when the storm intensification was at its lowest in this series, 38.49 kt. Table II gives the day-time and intensities of the eleven cases studied.

Table II

Day-Time	Intensity (kt)	Ratio	Csc
238.14	38.49	2 (6)	1.6
.22	47.03	3 (10)	2.03
239.06	57.83	-	1.45
.14	71.15	3 (8-10)	1.48
.22	91.72	1.5 (8)	1.43
240.06	114.91	4 (12)	1.65
.14	128.98	-	1.55
.22	125.43	-	2.67
241.22	122.50	-	1.63
242.22	130.31	-	1.86

All of the time intervals are of eight hour durations with the exception of the last two times in the table. The ratio is the value of the primary peak

divided by the value of the secondary peak where there is a bimodal distribution in the spectral analysis. With the exception of 239.06, where a bimodal distribution did not appear, the entire period of intensification was characterized by a strong secondary peak in the vicinity of wave numbers 8-10.

The figures in parentheses indicate the wave number of the secondary peak. The general trend is for the secondary peak to migrate from 6 outward toward 12 as the storm intensifies. The period of maximum intensification occurs between 239.14 and 240.06, during which time the storm doubles in strength from 71.15 to 114.91. Figure 24, 239.22, with an intensity of 91.72 and a ratio of 4 shows both strong values in waves numbered one and two, evident in the illustration (Fig 24) and also in wave number 8.

During this period of intensification, the inflow cosecant hovered around 1.45. From earlier analysis the cosecant of the inflow angle should give a rough indication of where the maximum in the spiral spectrum should occur. The presence of a secondary peak indicates a strong local pressure torque due to the asymmetries. This pressure torque is not independent of radius, causing strong interior torques in the storm, possibly preparatory to the creation of a core regime, complete with eye.

The eye exists throughout the whole series, so that in this case there is possibly only intensification and concentration of the storm rather than a specific regime change.

The storm levels out on 240.14 at 128.98. The secondary peak disappears at this time, and the storm becomes virtually steady-state.

4. Conclusions

From Table II it is evident that intensifying hurricanes may be identified with a secondary maximum in their spiral spectrum. The inflow cosecant becomes smallest of all in this period, about 1.45. The achievement of the slowly varying state is characterized by relaxation of the the inflow cosecant and the jump in the ratio of the primary to secondary peaks in the spiral spectrum.

The behavior of the eye and the placement of the spiral center does not seem correlated with the intensification of the storm. Theoretical influence of the spiral asymmetric pressure field seems correlated with the storm's behavior shown both in the spectral analysis and observation of the actual bands appearing in the satellite representations.

Prediction of hurricane intensification may be possible by observation of spectral bimodality. Obviously one case study does not make a trend, but it would be worth while to pursue the relevance of this phenomenon in other storms. Quite possibly, this would include the length of the individual bands, as suggested by Nicholson (1983), but which is not actually measured in this study.

REFERENCES

Cook, John, 1984: A Spiral Analysis Technique for Monitoring and Predicting Tropical Cyclone Intensity Using Satellite Data. NAVENVPREDRSCHFAC TR84-01, 100 pp.

Fett, Robert W. and Walter A. Bohen, 1981: Navy Tactical Applications Guide. Volume 3, North Atlantic and Mediterranean Weather Analysis and Forecast Applications, Naval Environmental Prediction Research Facility, Technical Report 80-07.

Nicholson, Francis H., 1983: A General Field Theory for Vortex Structure and Interaction, Office of Naval Research Report N00014-80-C-0026.

APPENDIX

FIGURES 9 - 28

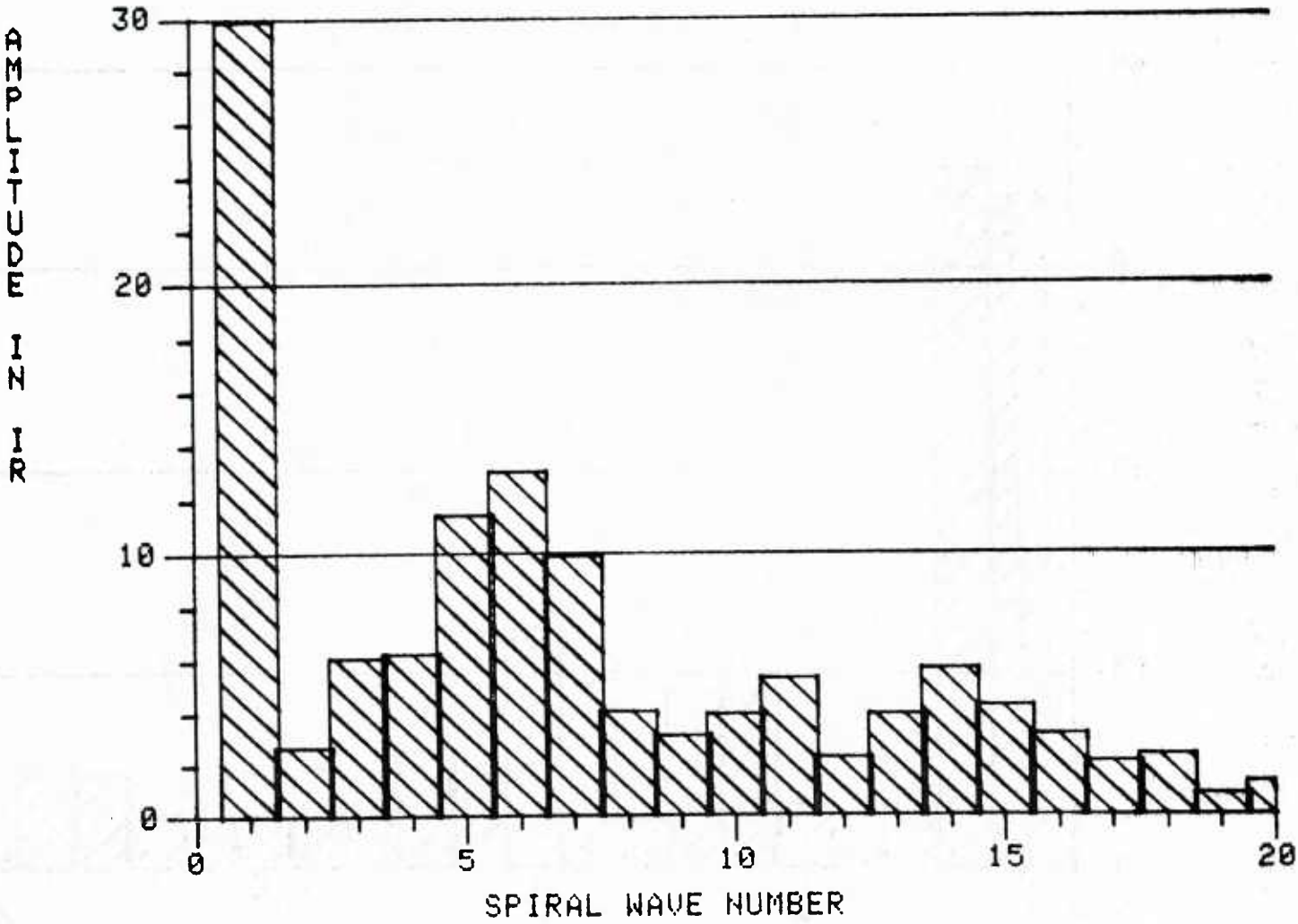

Fig. 9 Histogram of spiral band amplitude vs. wave number for Hurricane David 14Z 24 AUG 79 (Julian date 238.14).

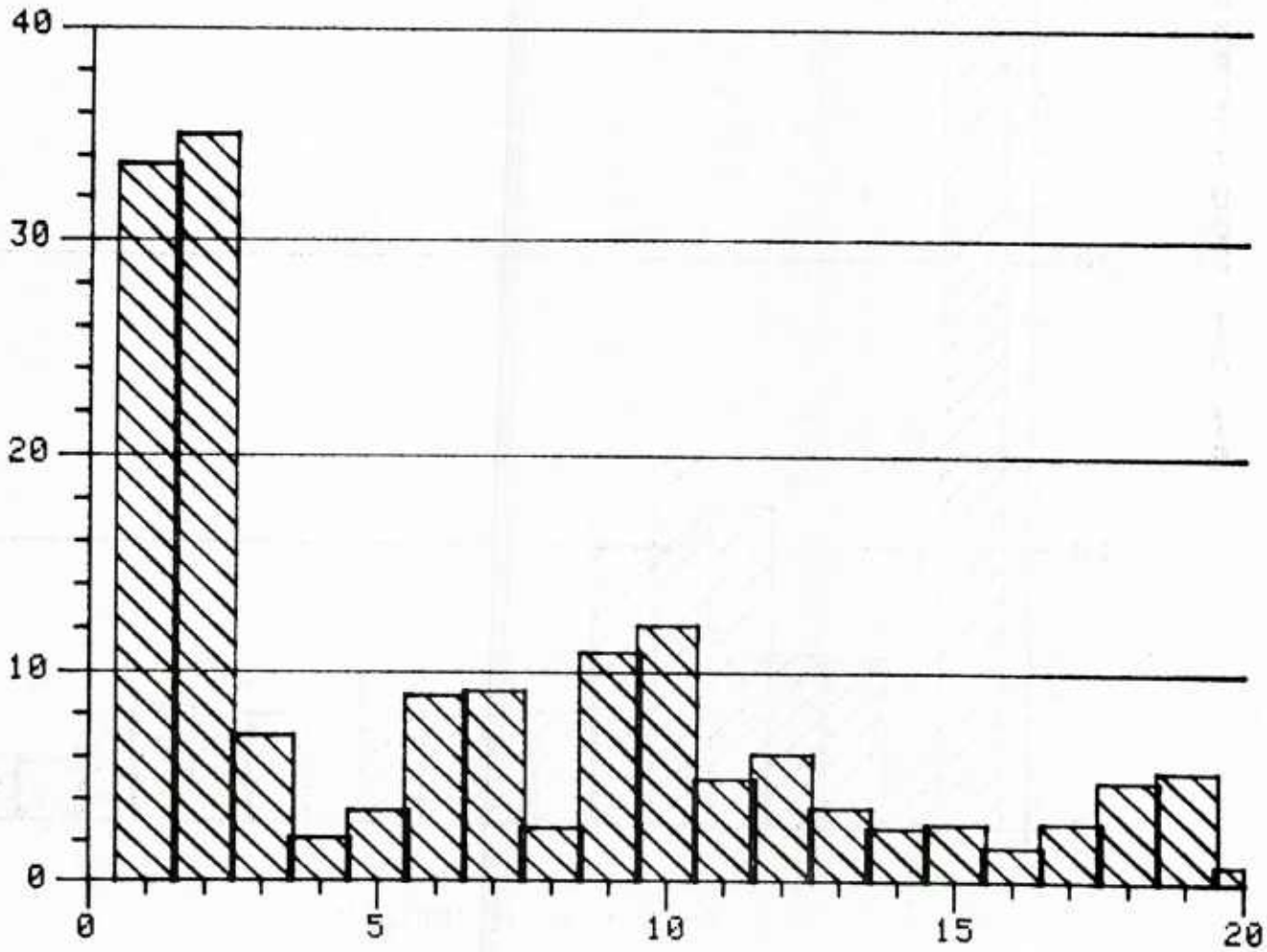

Fig. 10 Histogram of spiral band amplitude vs. wave number for Hurricane David 22Z 24 AUG 79 (Julian date 238.22).

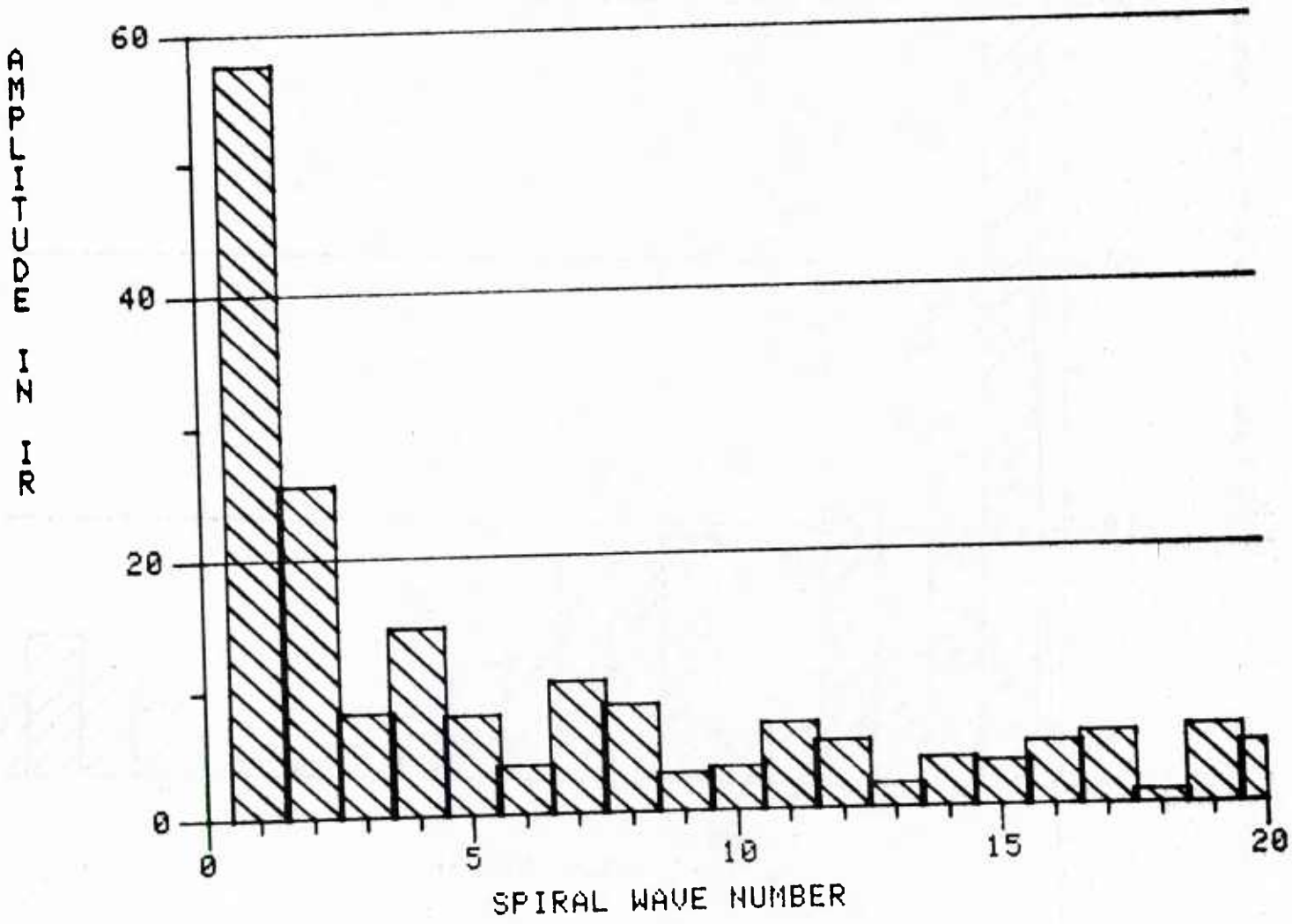

Fig.11 Histogram of spiral band amplitude vs. wave number for Hurricane David 06Z 25 AUG 79 (Julian date 239.06).

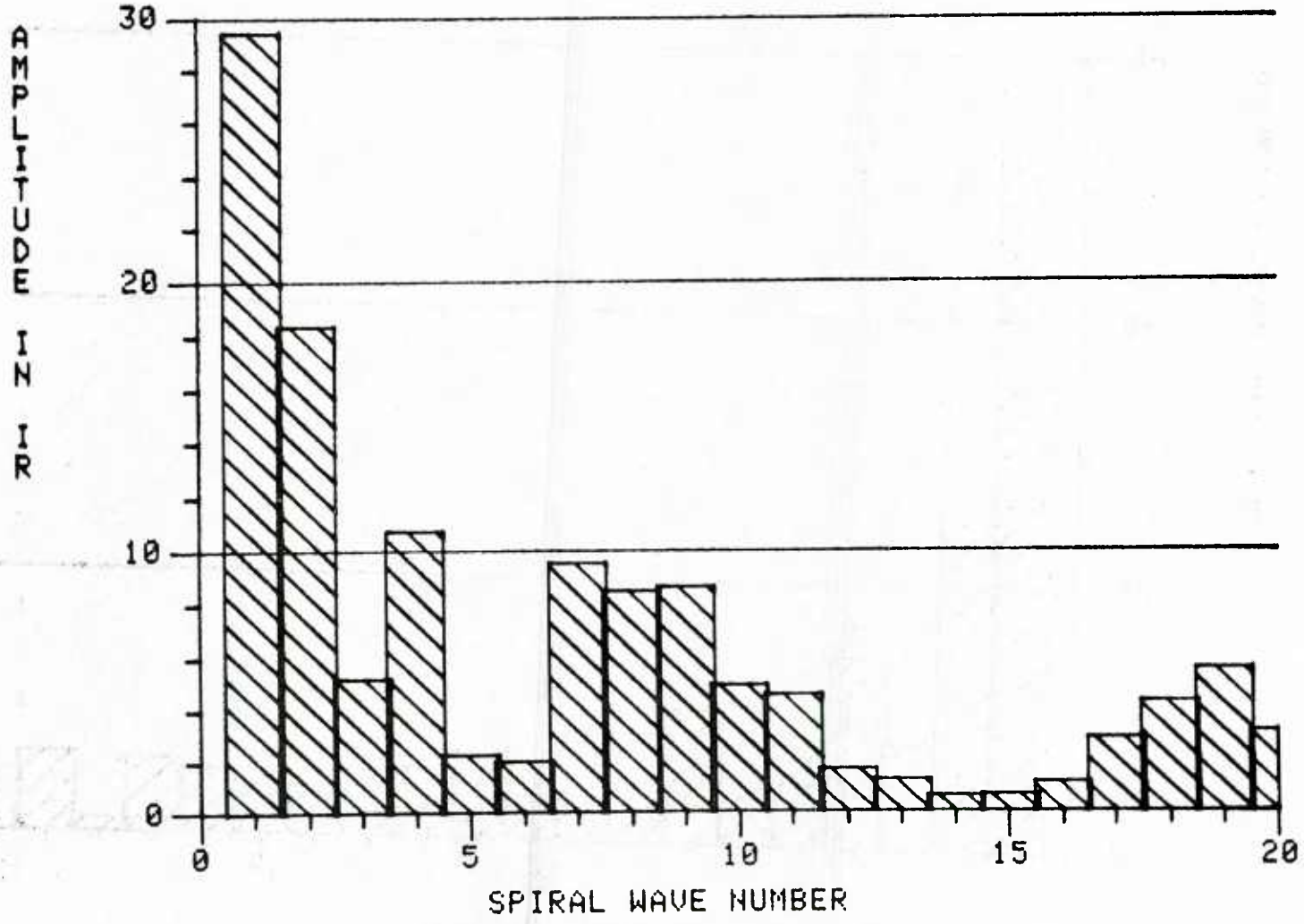

Fig. 12 Histogram of spiral band amplitude vs. wave number for Hurricane David 14Z 25 AUG 79 (Julian date 239.14).

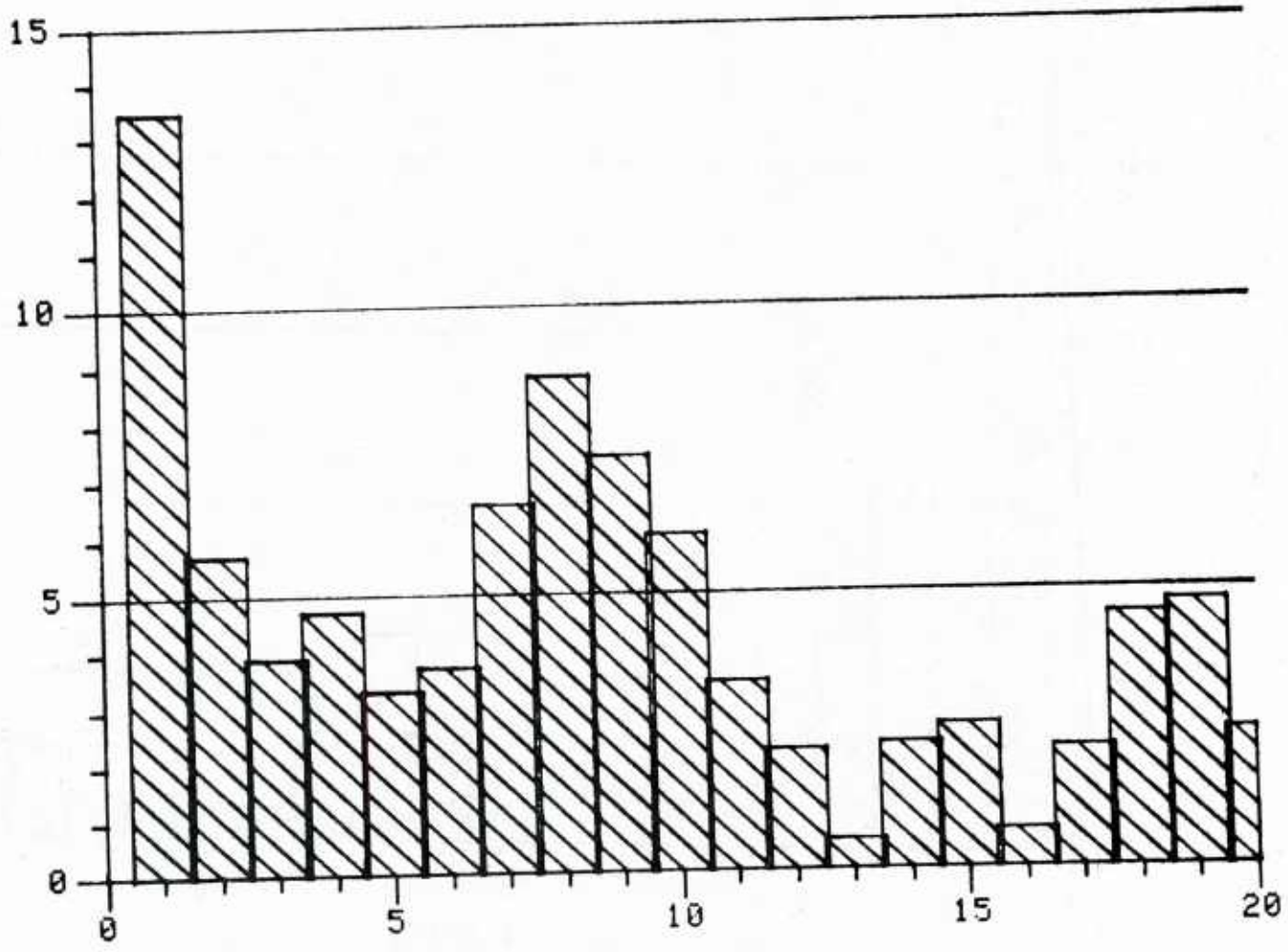

Fig. 13 Histogram of spiral band amplitude vs. wave number for Hurricane David 22Z 25 AUG 79 (Julian date 239.22).

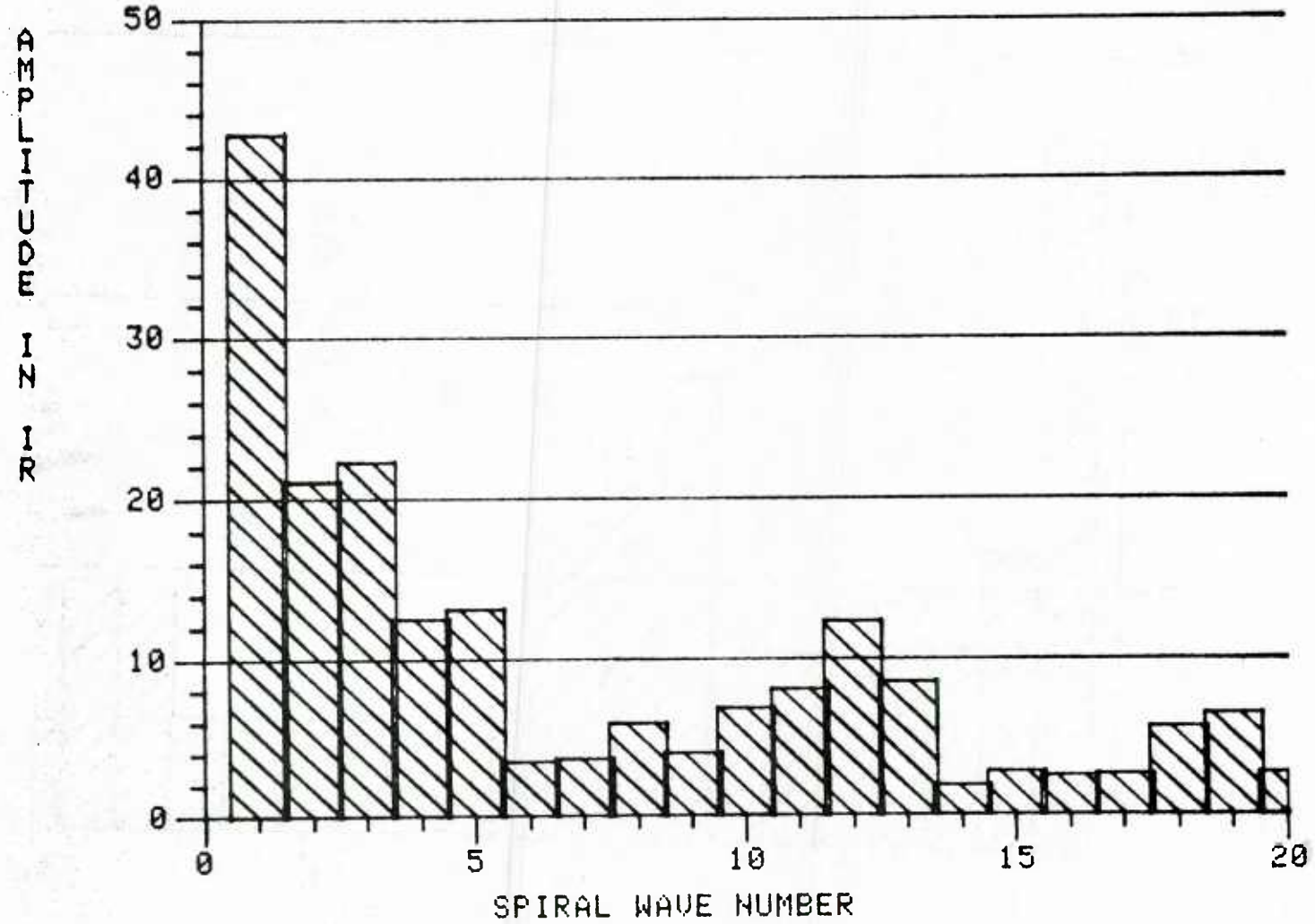

Fig. 14 Histogram of spiral band amplitude vs. wave number for Hurricane David 06Z 26 AUG 79 (Julian date 240.06).

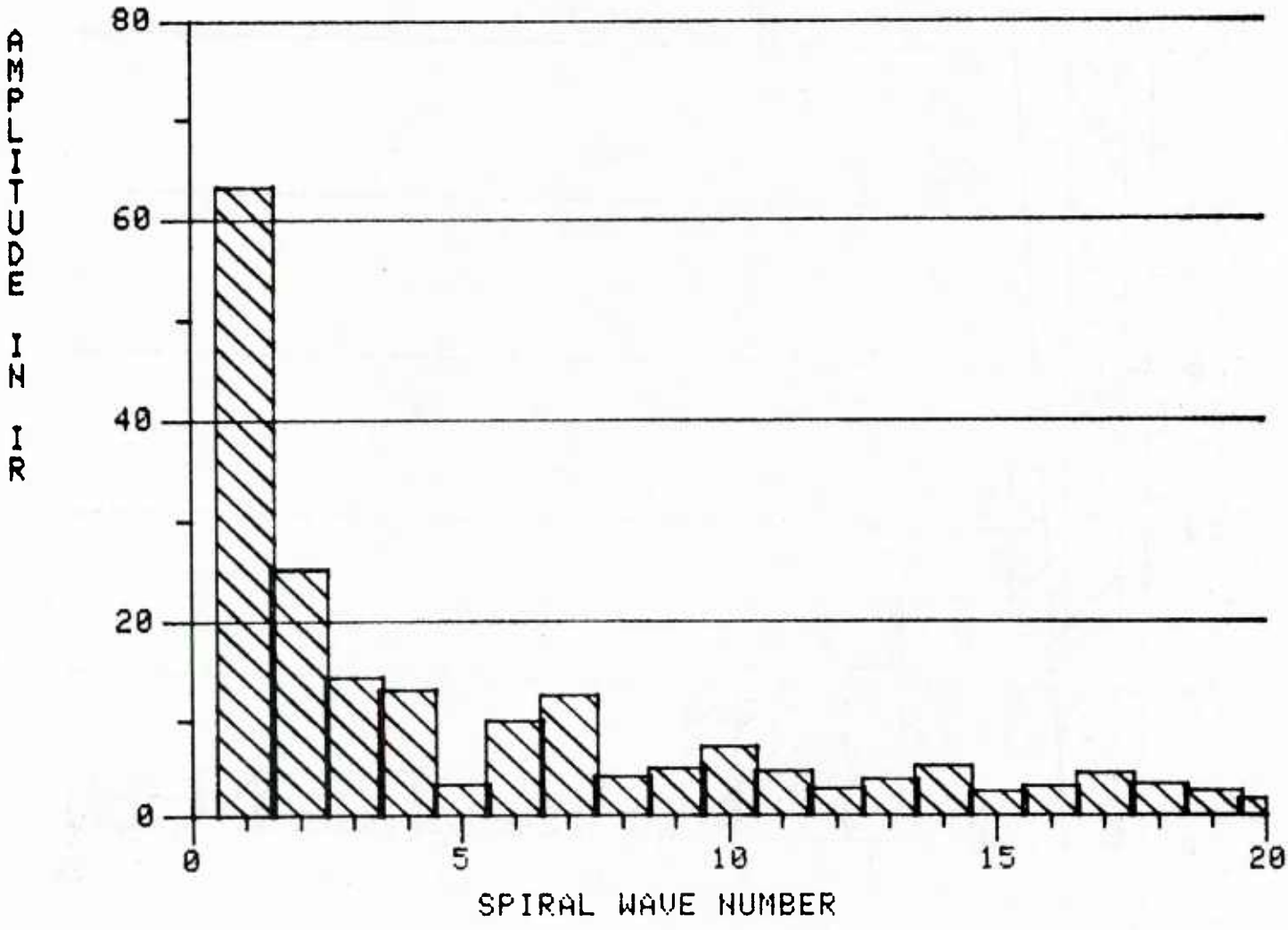

Fig. 15 Histogram of spiral band amplitude vs. wave number for Hurricane David 14Z 26 AUG 79 (Julian date 240.14).

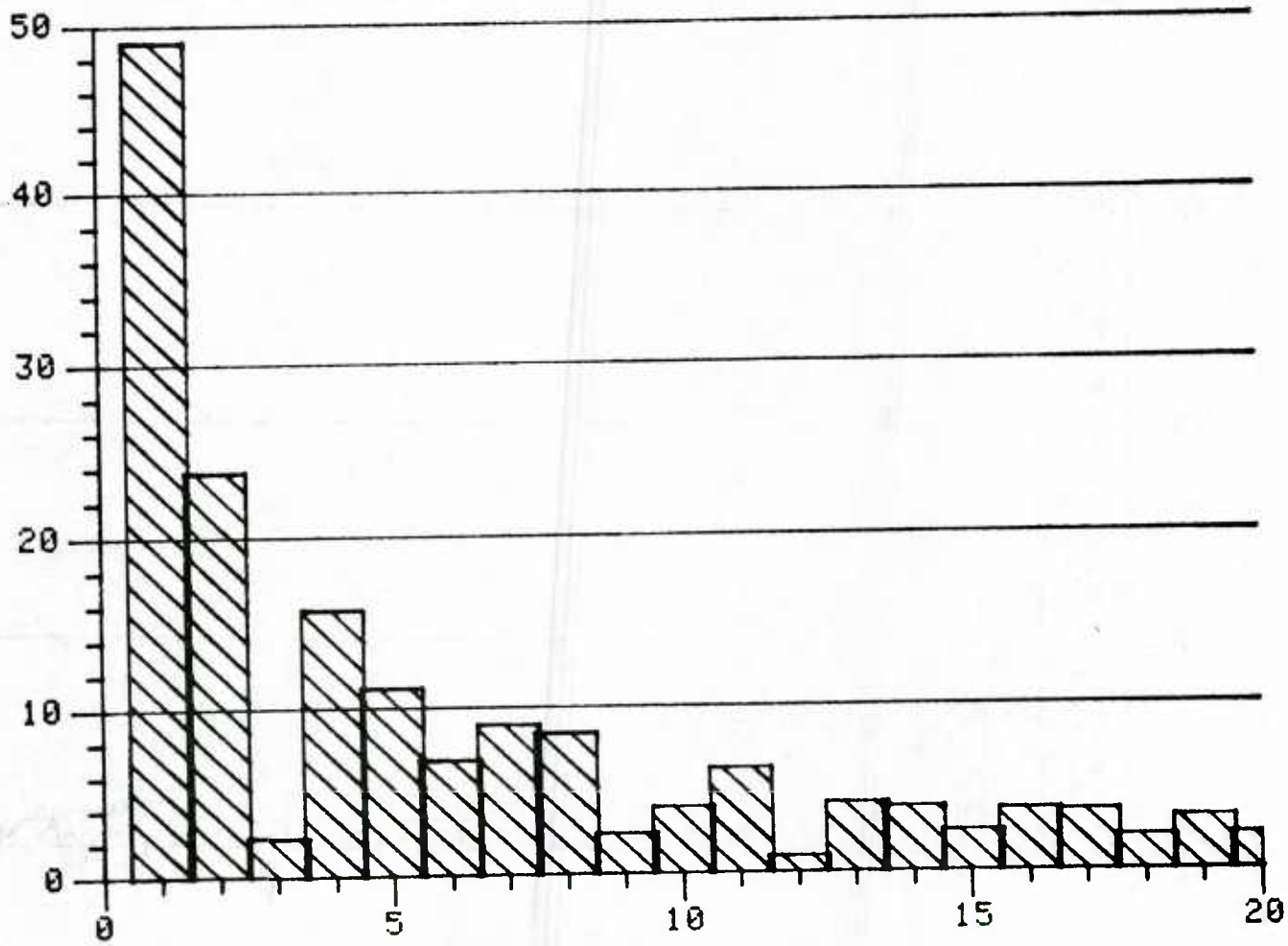

Fig. 16 Histogram of spiral band amplitude vs. wave number for Hurricane David 22Z 26 AUG 79 (Julian date 240.22).

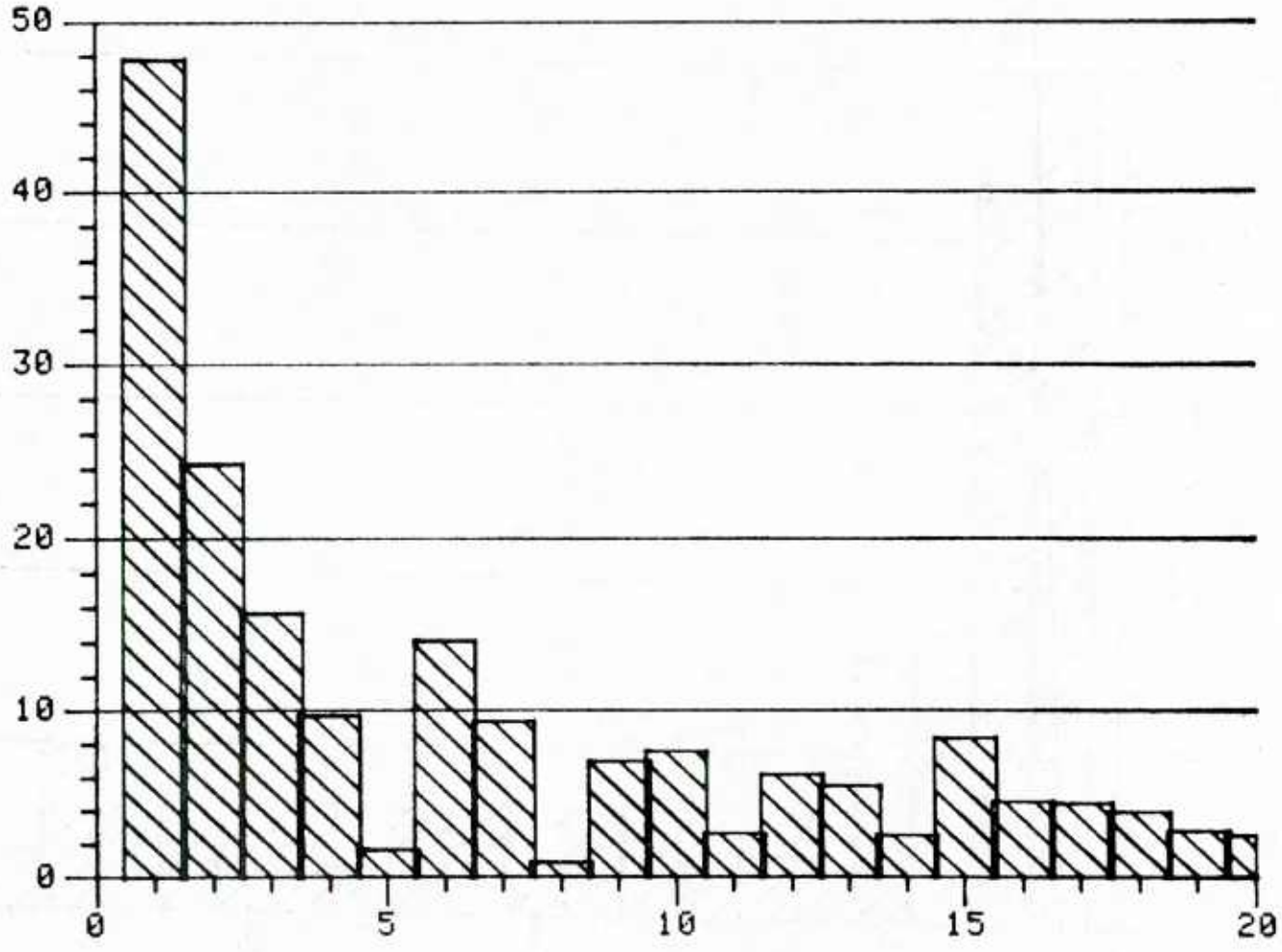

Fig. 17 Histogram of spiral band amplitude vs. wave number for Hurricane David 22Z 27 AUG 79 (Julian date 241.22).

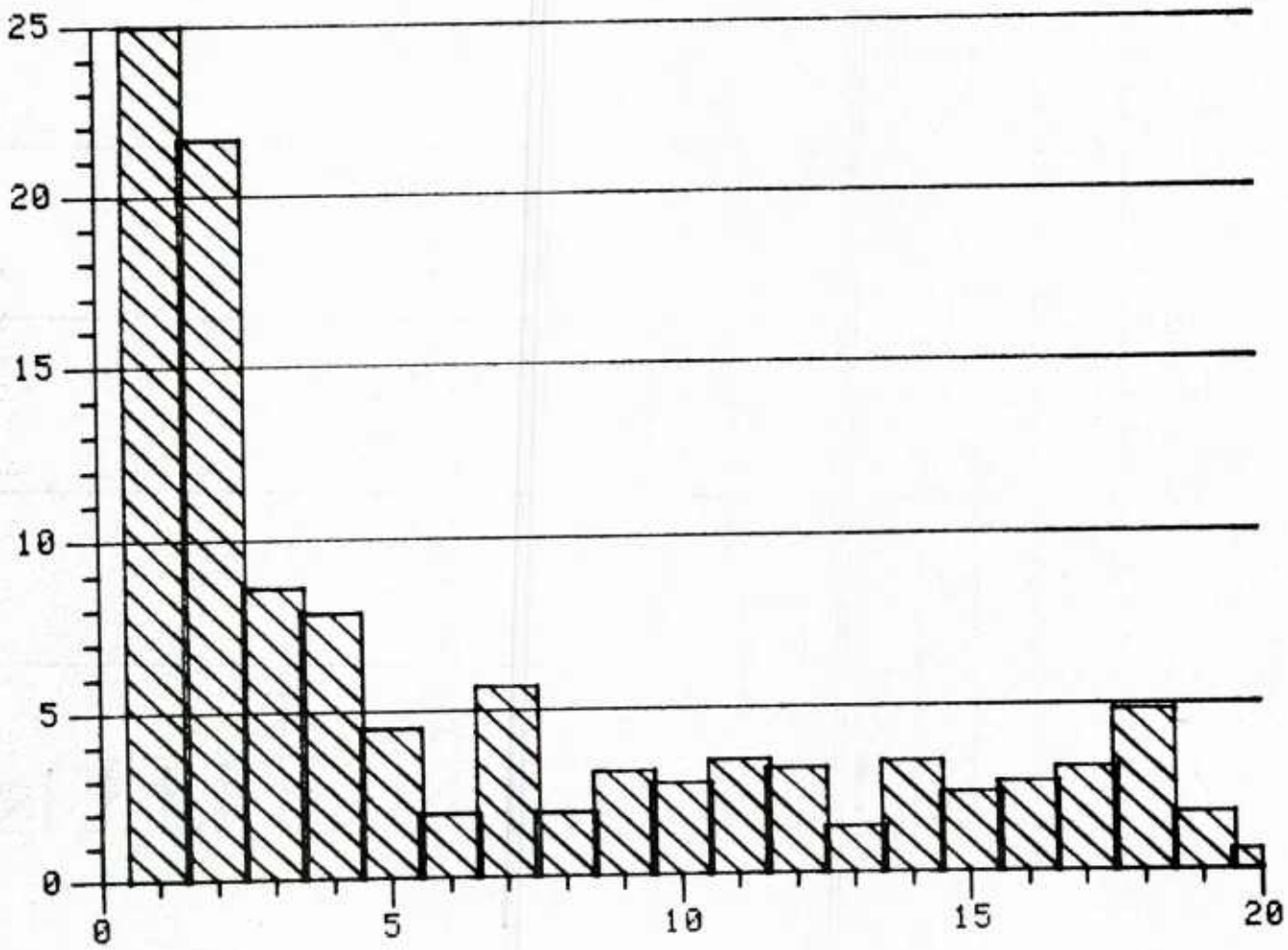

Fig. 18 Histogram of spiral band amplitude vs. wave number for Hurricane David 22Z 28 AUG 79 (Julian date 242.22).

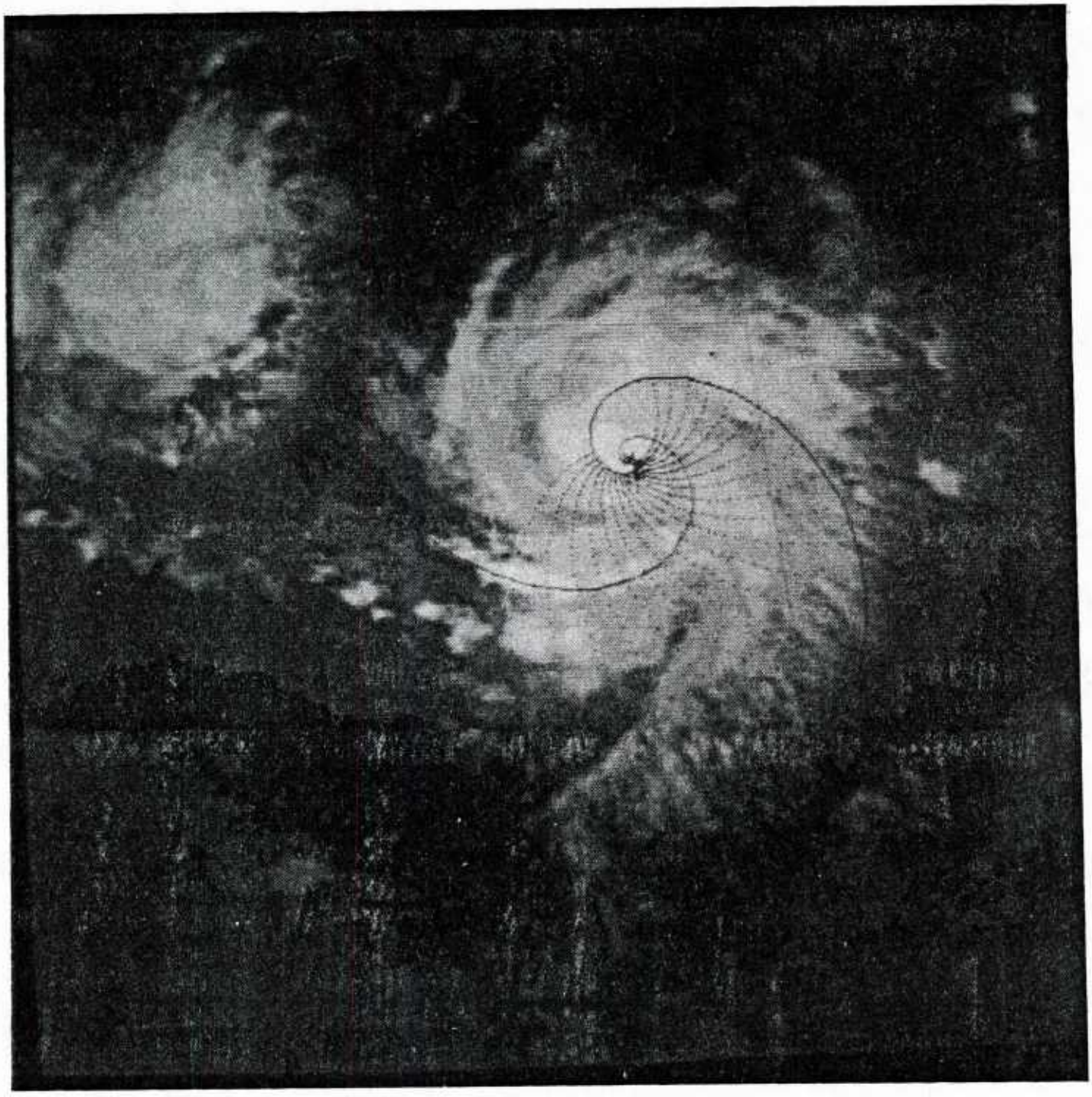

Fig. 19 Hurricane David 14Z 24 AUG 79 (Julian date 238.14).

Fig. 20 Hurricane David 22Z 24 AUG 79 (Julian date 238.22).

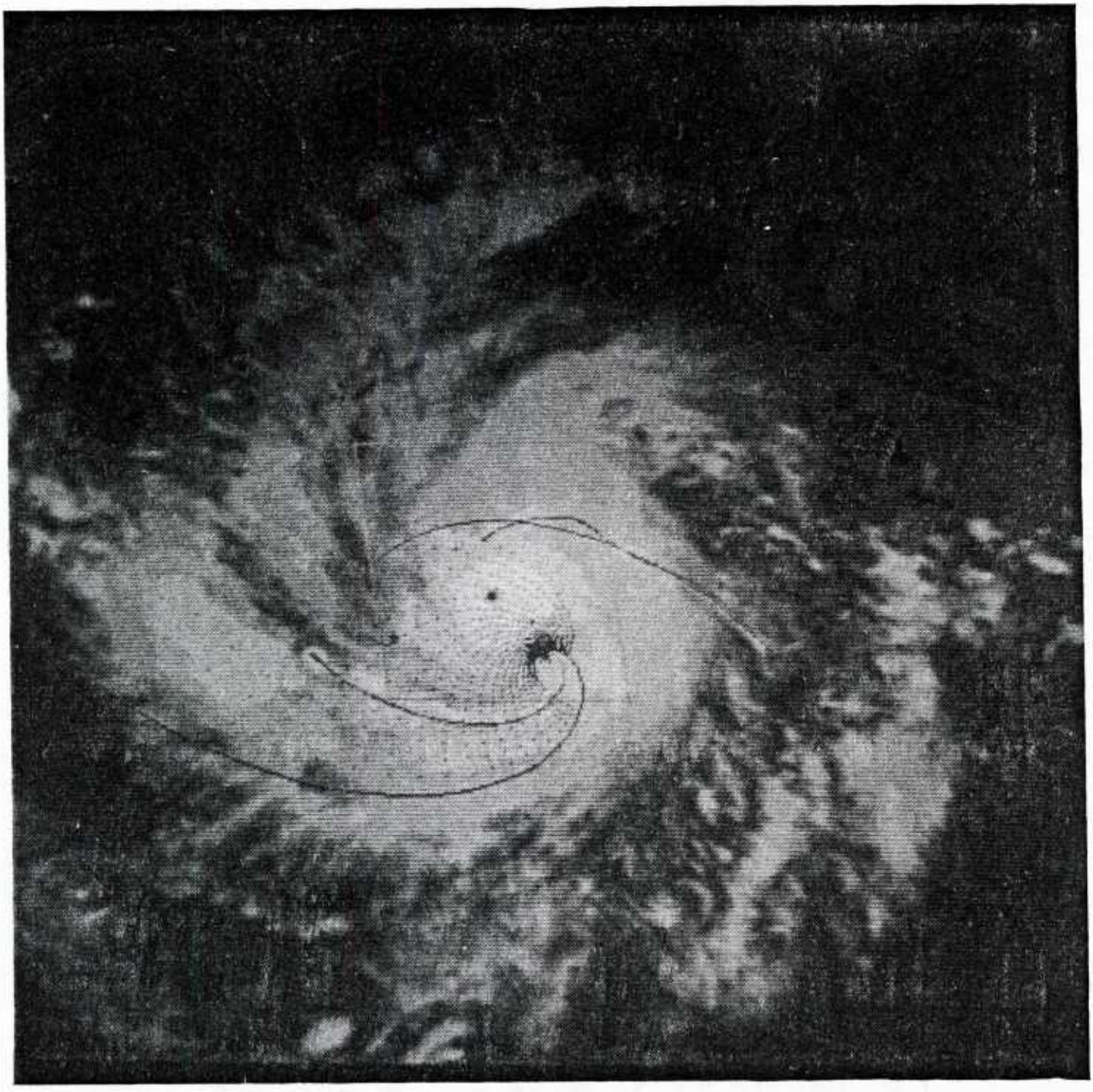

Fig. 21 Hurricane David 06Z 25 AUG 79 (Julian date 239.06).

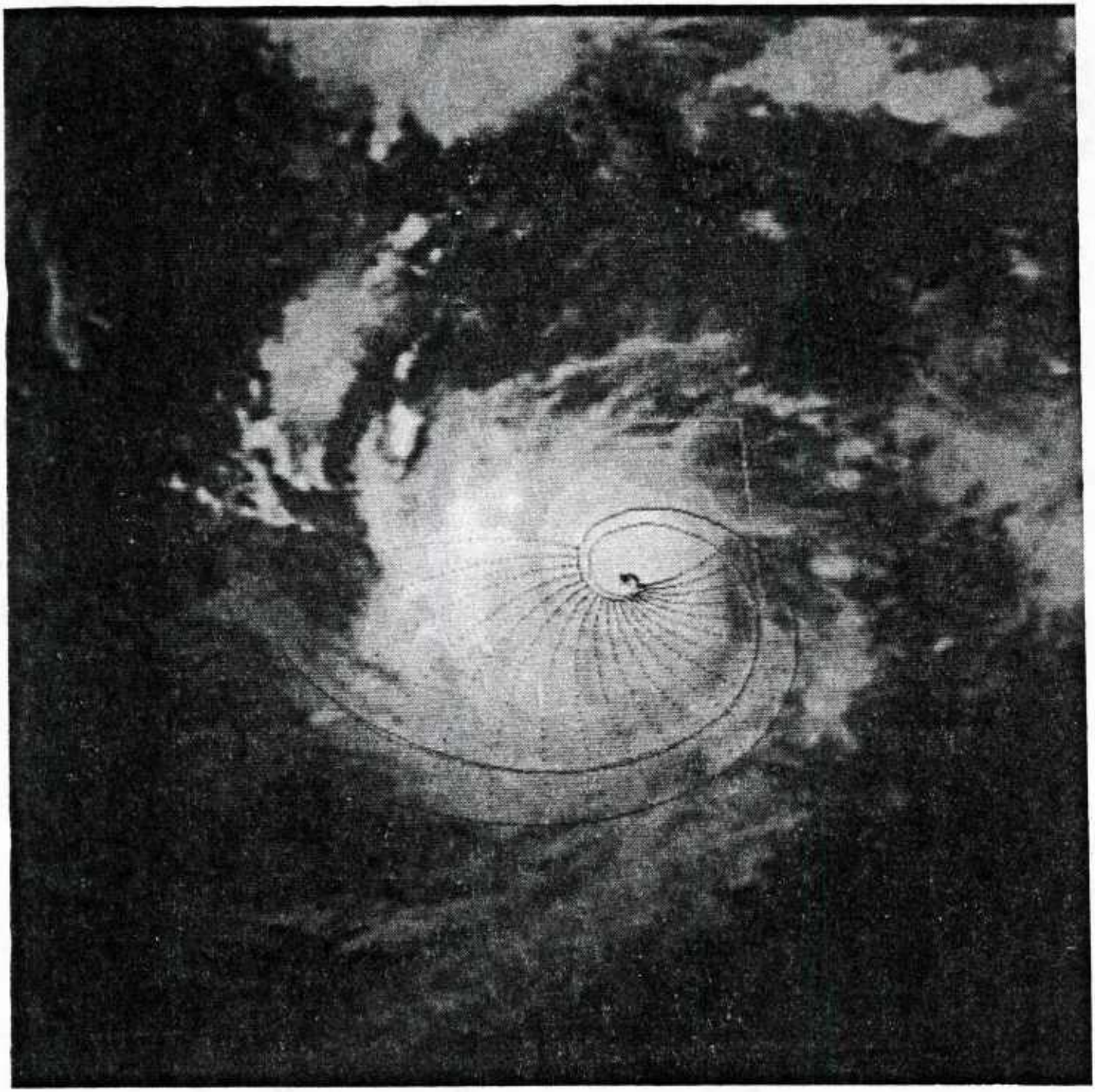

Fig. 22 Hurricane David 14Z 25 AUG 79 (Julian date 239.14).

Fig. 23 Hurricane David 22Z 25 AUG 79 (Julian date 239.22).

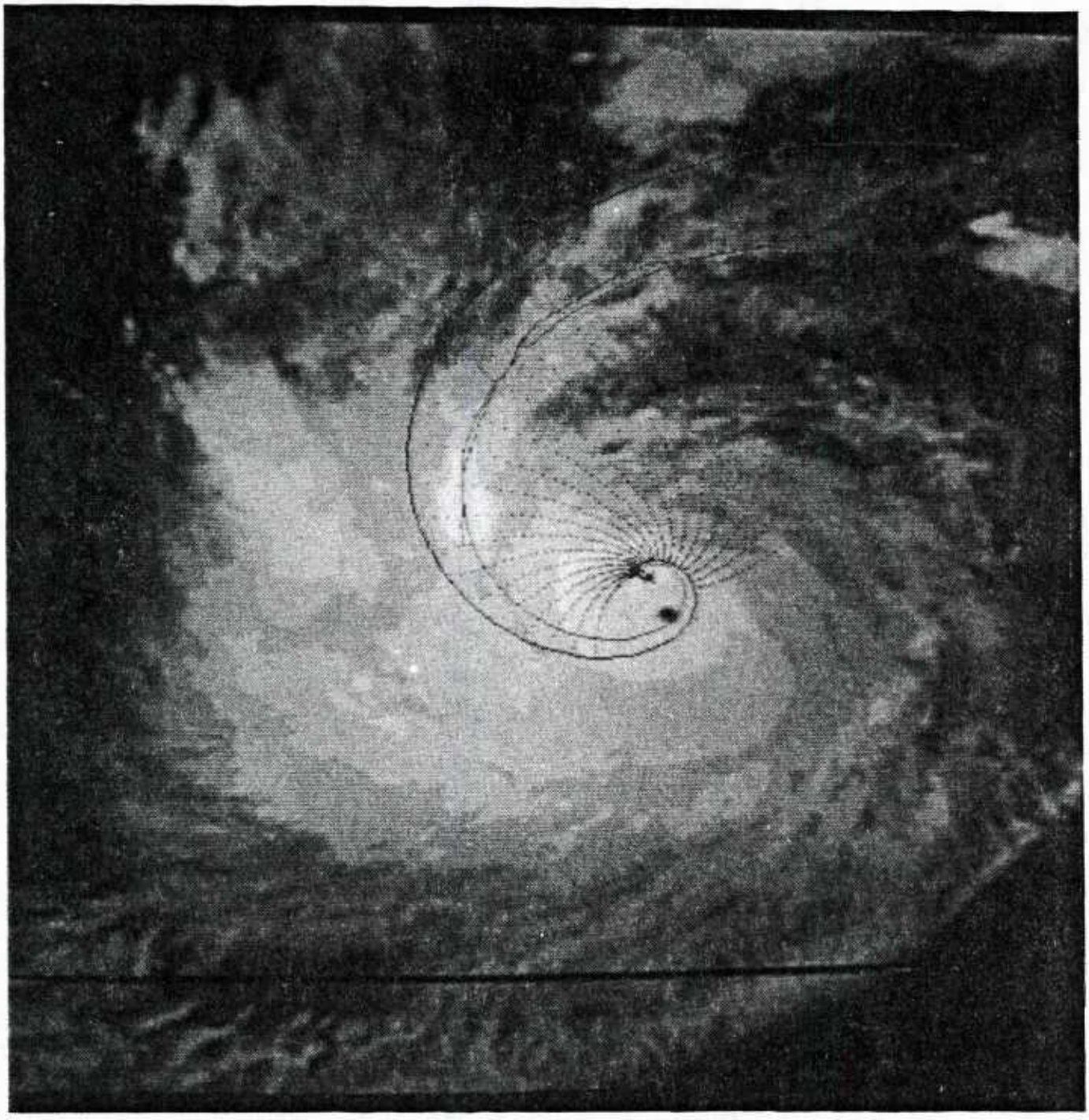

Fig. 24 Hurricane David 06Z 26 AUG 79 (Julian date 240.06).

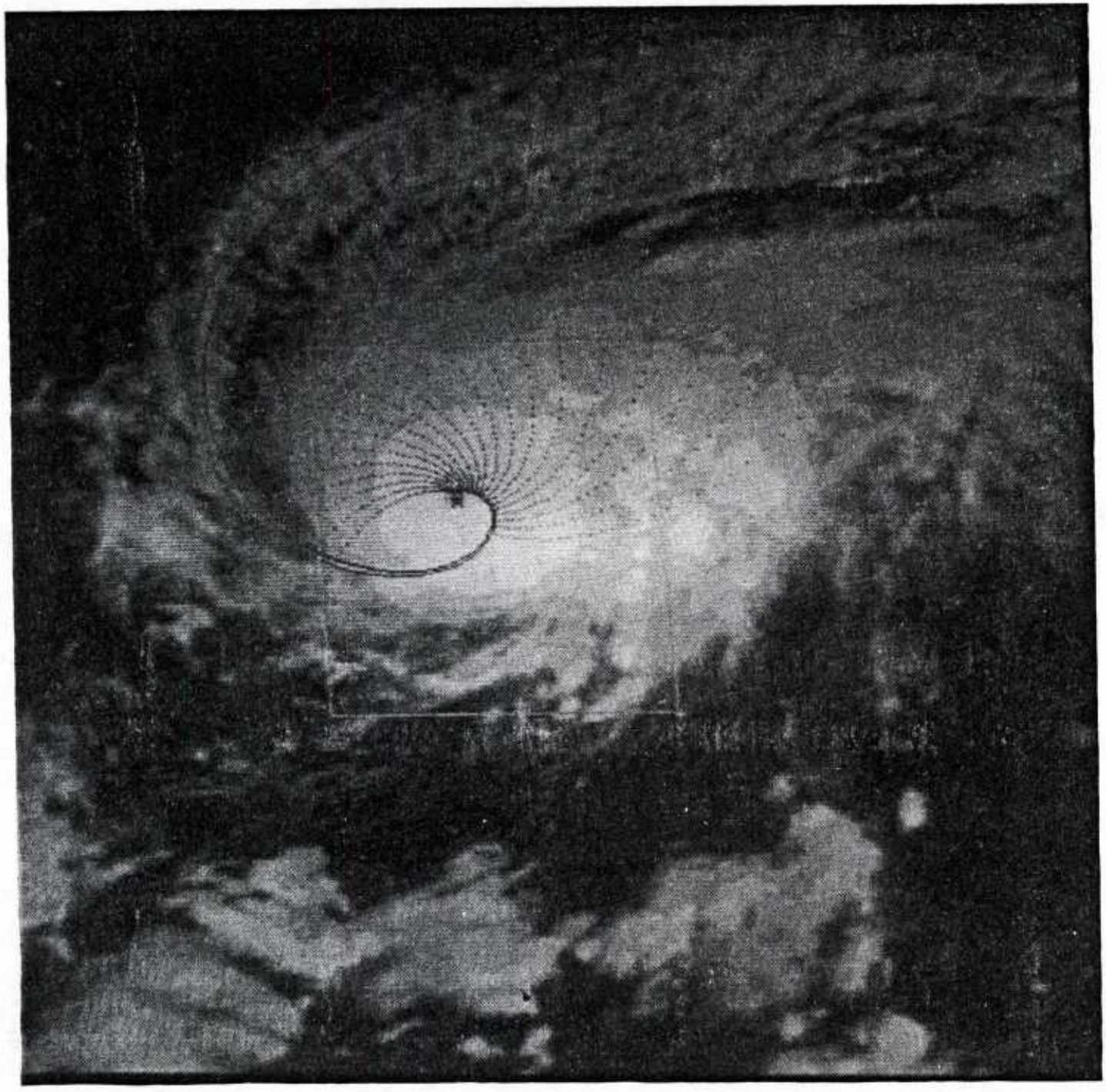

Fig. 25 Hurricane David 14Z 26 AUG 79 (Julian date 240.14).

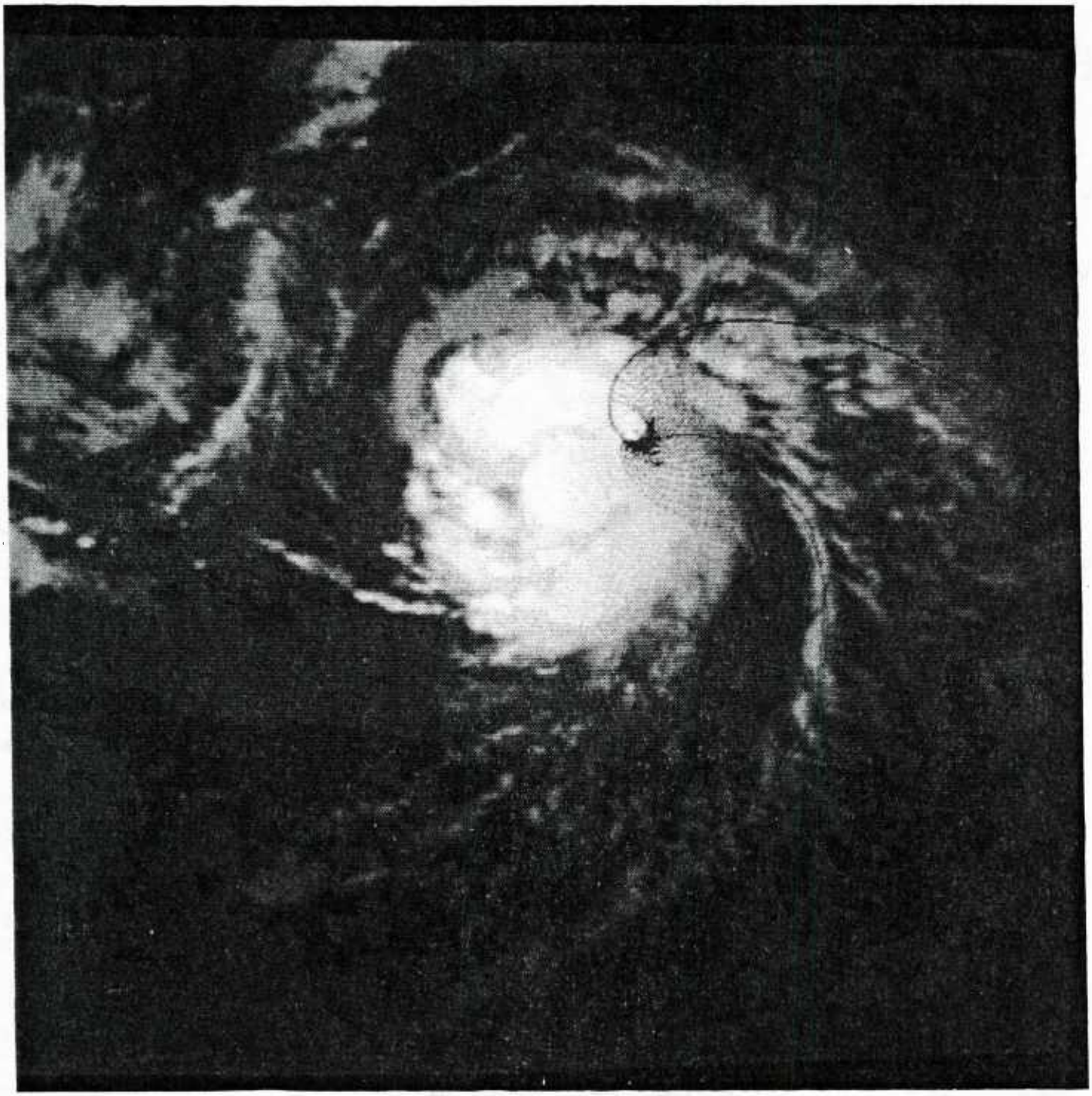

Fig. 26 Hurricane David 22Z 26 AUG 79 (Julian date 240.22).

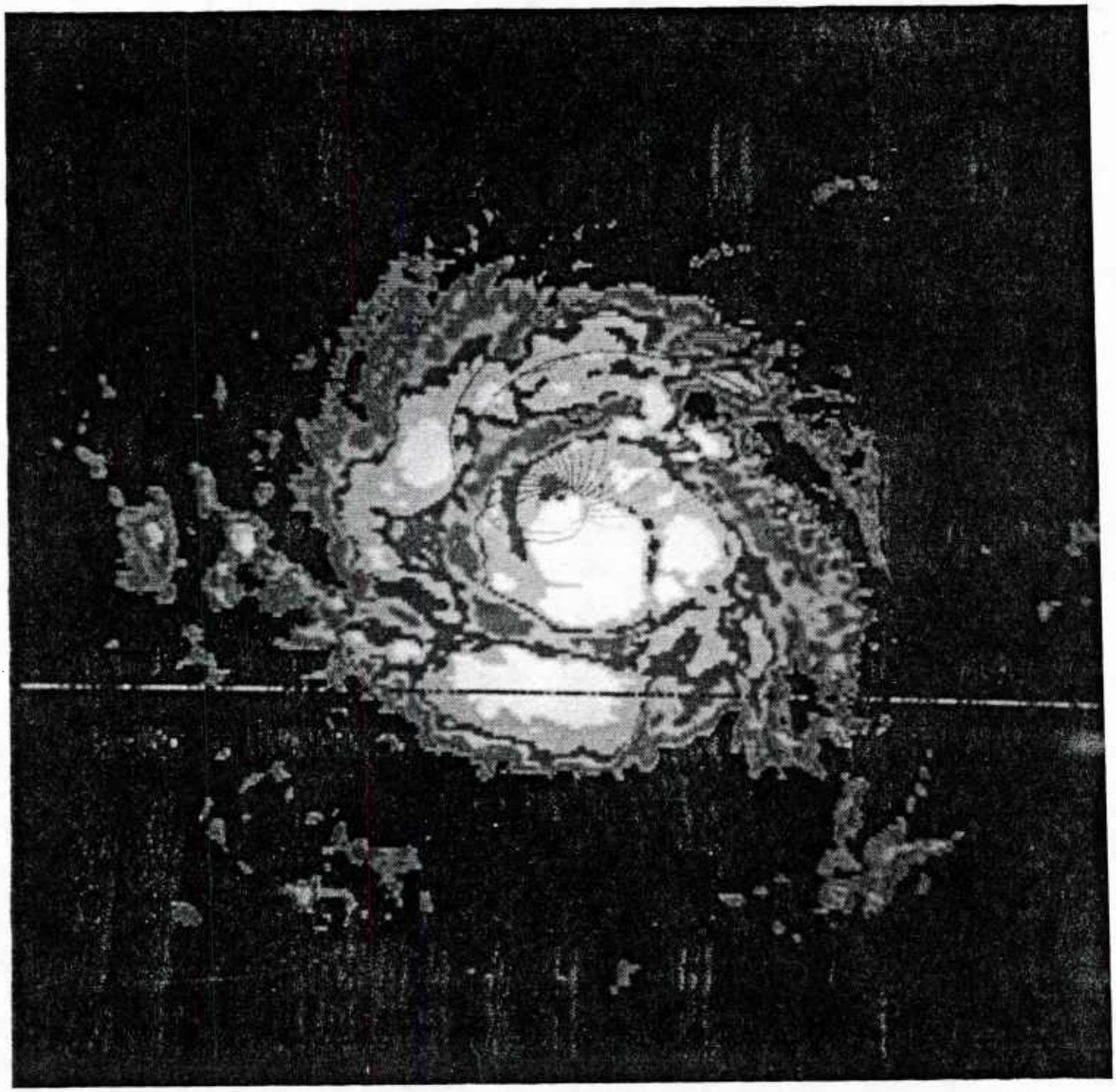

Fig. 27 Hurricane David 22Z 27 AUG 79 (Julian date 241.22).

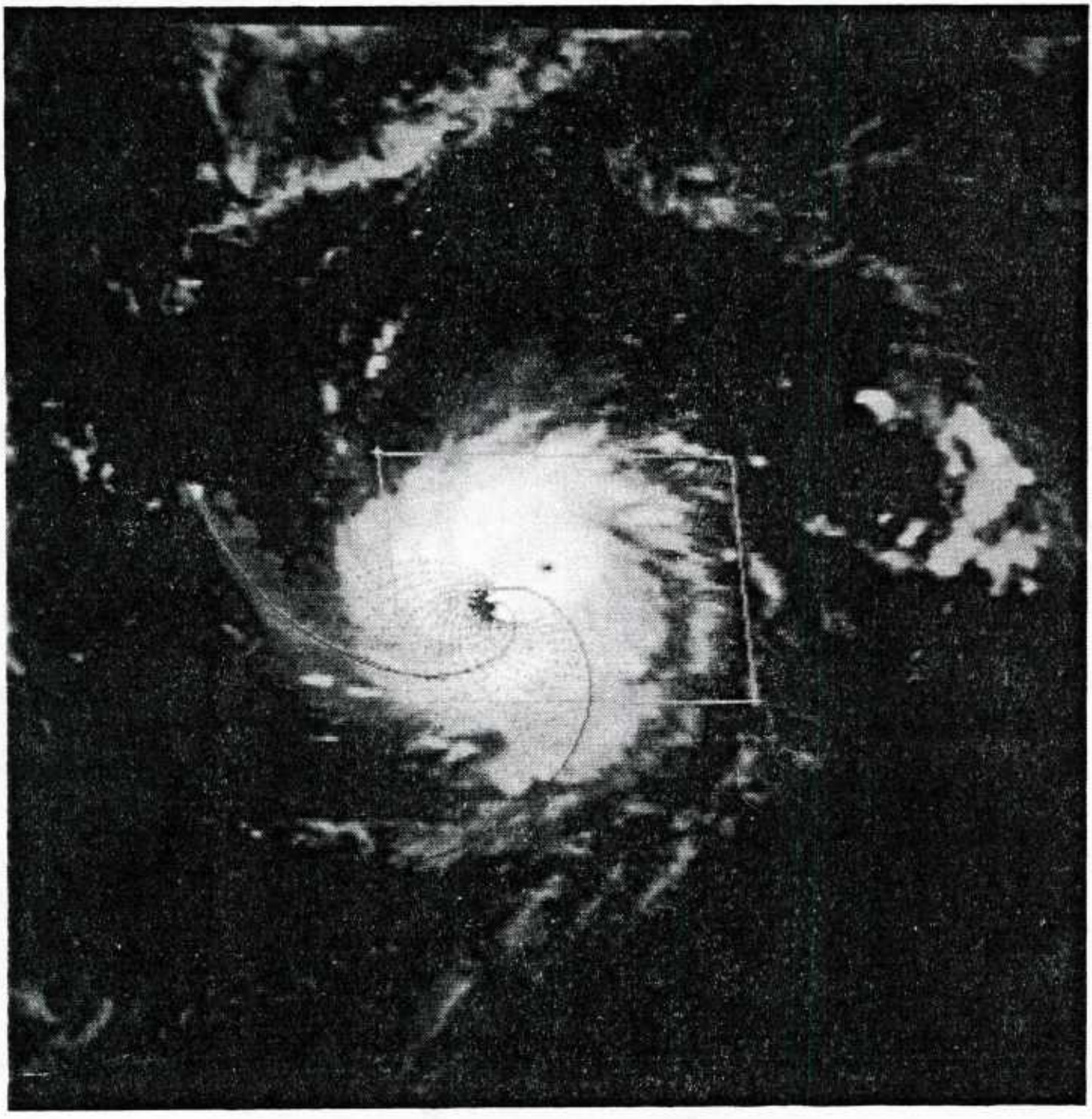

Fig. 28 Hurricane David 22Z 28 AUG 79 (Julian date 242.22).

COMMANDER IN CHIEF
U.S. ATLANTIC FLEET
ATTN: FLT METEOROLOGIST
NORFOLK, VA 23511

COMMANDER IN CHIEF
U.S. ATLANTIC FLEET
ATTN: NSAP SCIENCE ADVISOR
NORFOLK, VA 23511

COMTHIRDFLT
ATTN: FLT METEOROLOGIST
PEARL HARBOR, HI 96860

COMSEVENTHFLT
ATTN: FLT METEOROLOGIST
FPO SAN FRANCISCO 96601

COMTHIRDFLT
ATTN: NSAP SCIENCE ADVISOR
PEARL HARBOR, HI 96860

COMSEVENTHFLT
ATTN: NSAP SCIENCE ADVISOR
BOX 167
FPO SEATTLE 98762

CHIEF OF NAVAL RESEARCH (2)
LIBRARY SERVICES, CODE 784
BALLSTON TOWER #1
800 QUINCY ST.
ARLINGTON, VA 22217

COMMANDING OFFICER
NAVWESTOCEANCEN
BOX 113
PEARL HARBOR, HI 96860

COMMANDING OFFICER
NAVEASTOCEANCEN
MCADIE BLDG. (U-117)
NAVAL AIR STATION
NORFOLK, VA 23511

COMMANDING OFFICER
U.S. NAVOCEANCOMCEN
BOX 12, COMNAVMARIANAS
FPO SAN FRANCISCO 96630

NAVAL POSTGRADUATE SCHOOL
METEOROLOGY DEPT.
MONTEREY, CA 93943

LIBRARY
NAVAL POSTGRADUATE SCHOOL
MONTEREY, CA 93943

PRESIDENT
NAVAL WAR COLLEGE
ATTN: GEOPHYSICS OFFICER
NEWPORT, RI 02840

COMMANDER (2)
NAVAIRSYSCOM
ATTN: LIBRARY (AIR-7226)
WASHINGTON, DC 20361

COMMANDER
NAVAIRSYSCOM (AIR-330)
WASHINGTON, DC 20361

DIRECTOR, CENTRAL PACIFIC
HURRICANE CENTER, NWS, NOAA
HONOLULU, HI 96819

USAFETAC/TS
SCOTT AFB, IL 62225

3350TH TECH. TRNG GROUP
TTGU/2/STOP 623
CHANUTE AFB, IL 61868

AFGWC/DAPL
OFFUTT AFB, NE 68113

3 WW/DN
OFFUTT AFB, NE 68113

COMMANDING OFFICER
U.S. ARMY RESEARCH OFFICE
ATTN: GEOPHYSICS DIV.
P.O. BOX 12211
RESEARCH TRIANGLE PARK, NC
27709

DIRECTOR (12)
DEFENSE TECH. INFORMATION
CENTER, CAMERON STATION
ALEXANDRIA, VA 22314

DIRECTOR
NATIONAL HURRICANE CENTER
NOAA, GABLES ONE TOWER
1320 S. DIXIE HWY
CORAL GABLES, FL 33146

METEOROLOGIST IN CHARGE
WEA. SERV. FCST. OFFICE, NOAA
660 PRICE AVE.
REDWOOD CITY, CA 94063

DIRECTOR
FEDERAL EMERGENCY MANAGEMENT
AGENCY (FEMA)
WASHINGTON, DC 20472

COLORADO STATE UNIVERSITY (2)
ATTN: DR. WILLIAM GRAY
ATMOSPHERIC SCIENCES DEPT.
FT. COLLINS, CO 80523

INSTITUTE FOR STORM RESEARCH
UNIVERSITY OF ST. THOMAS
3600 MT. VERNON
HOUSTON, TX 77006

DIRECTOR, JTWC (5)
BOX 17
FPO SAN FRANCISCO 96630

LIBRARY, AUSTRALIAN NUMERICAL
METEOROLOGY RESEARCH CENTER
P.O. BOX 5089A
MELBUORNE, VICTORIA,3001
AUSTRALIA

MARITIME METEOROLOGY DIV.
JAPAN METEOROLOGICAL AGENCY
OTE-MACHI 1-3-4 CHIYODA-KU
TOKYO, JAPAN

DIRECTOR, TYPHOON MODERATION
RSCH. & DEVEL. OFFICE, PAGASA
MINISTRY OF NATIONAL DEFENSE
1424 QUEZON AVE.
QUEZON CITY, PHILIPPINES

CHIEF ATMOS. SCIENCES DIV.
WORLD METEORO. ORGANIZATION
P.O. BOX 5
GENEVA 20, SWITZERLAND